

Master thesis : Development of Methodology for Predicting Marine Vessel Turning Radius with Overset Grid Technique using CFD Solver

Auteur : Andalib, Abu Afree

Promoteur(s) : 18524

Faculté : Faculté des Sciences appliquées

Diplôme : Master : ingénieur civil mécanicien, à finalité spécialisée en "Advanced Ship Design"

Année académique : 2021-2022

URI/URL : <http://hdl.handle.net/2268.2/16561>

Avertissement à l'attention des usagers :

Tous les documents placés en accès ouvert sur le site le site MatheO sont protégés par le droit d'auteur. Conformément aux principes énoncés par la "Budapest Open Access Initiative"(BOAI, 2002), l'utilisateur du site peut lire, télécharger, copier, transmettre, imprimer, chercher ou faire un lien vers le texte intégral de ces documents, les disséquer pour les indexer, s'en servir de données pour un logiciel, ou s'en servir à toute autre fin légale (ou prévue par la réglementation relative au droit d'auteur). Toute utilisation du document à des fins commerciales est strictement interdite.

Par ailleurs, l'utilisateur s'engage à respecter les droits moraux de l'auteur, principalement le droit à l'intégrité de l'oeuvre et le droit de paternité et ce dans toute utilisation que l'utilisateur entreprend. Ainsi, à titre d'exemple, lorsqu'il reproduira un document par extrait ou dans son intégralité, l'utilisateur citera de manière complète les sources telles que mentionnées ci-dessus. Toute utilisation non explicitement autorisée ci-avant (telle que par exemple, la modification du document ou son résumé) nécessite l'autorisation préalable et expresse des auteurs ou de leurs ayants droit.



Universität
Rostock



Traditio et Innovatio



SOLENT
UNIVERSITY
SOUTHAMPTON



Zachodniopomorski
Uniwersytet
Technologiczny
w Szczecinie



With the support of the
Erasmus+ Programme
of the European Union



Development of methodology for predicting marine vessel turning radius with overset grid technique using CFD solver

Abu Afree ANDALIB

Master Thesis

presented in partial fulfillment
of the requirements for the double degree:
"Advanced Ship Design" conferred by University of Liege
"Master of Marine Technology, specialized in Hydrodynamics and Ocean
Engineering" conferred by Ecole Centrale de Nantes

**Erasmus Mundus Joint Master Degree (EMJMD)
entitled as**

"EMSHIP+ Advanced design of ships and offshore structures"

EMJMD – Grant Agreement no 20191464, Edition 2020

Nantes, August 2022

Development of methodology for predicting marine vessel turning radius with overset grid technique using CFD solver

Abu Afree ANDALIB

Supervisor:

Nolwenn Huon de Kermadec, Marine Engineer, Mauric, 1 All. Baco, 44000 Nantes.

Board of Examiner:

Zhe Li, Maître de Conférences, Research Laboratory in Hydrodynamics, Energetics & Atmospheric Environment (LHEEA), Ecole Centrale de Nantes.

Lionel Gentaz, Professor, Fluid Mechanics and Energetics Department, Ecole Centrale de Nantes.

External Examiner:

Florin Pacuraru, Professor, Faculty of Naval Architecture, University of Galati.

This Thesis is Submitted for the degree of Master of Marine Technology
Department of Fluid Mechanics and Energetics
Ecole Centrale de Nantes

August 2022

Contents

List of Figures	iii
List of Tables.....	iv
Declaration of Authorship	v
Dedication	vi
Acknowledgement.....	vii
Abstract	viii
Chapter 1 Introduction	1
1.1 Problem Statement and Motivation	1
1.2 Formulation	2
1.3 Objective of the thesis	2
1.4 Scope of the thesis	3
Chapter 2 Literature	4
2.1 IMO, ITTC and Rulebooks	4
2.2 Equation of Motion	7
2.3 Proposed Numerical Model	16
2.3.1 Coordinate System and initial equation set	16
2.3.2 Mathematical Model.....	19
Chapter 3 Methodology, Simulation and Validation	27
3.1 CFD and Overset Mesh.....	27
3.2 Mesh and RANSE Solver.....	28
3.3 Meshing Methodology.....	28
3.3.1 Domains	28
3.3.2 Initial Cell Size	32
3.3.3 Mesh Adaptation Technique	33
3.3.4 Viscous Layer Addition	35
3.4 Simulation Phase	36
3.4.1 Acceleration Phase	36
3.4.2 Turning Circle Phase	37
3.4.3 Crash and Inertia Stop Phase	40
3.5 Result and Validation.....	41
3.5.1 Acceleration Phase Result and Graphics.....	41
3.5.2 Turning Circle Phase Result and Graphics.....	44
3.5.3 Comparison for 3 DOF and 6 DOF with Experimental Data.....	49
3.5.4 Post Processing Results.....	51

3.5.5 Critical Analysis	52
3.6 Challenges and Computation Error	53
Chapter 4 Conclusion and Recommendation	54
4.1 Conclusion	54
4.2 Limitations	54
4.3 Recommendations	55
Chapter 5 Reference	56
Appendices: Octave Code	A

List of Figures

Figure 1: A universal turning circle diagram	2
Figure 2: Moments and Rudder interaction in turning	8
Figure 3: Coordinate system.....	17
Figure 4: Body Transformation.....	18
Figure 5: Crash stop of a vessel.....	22
Figure 6: Time execution for stop order.....	24
Figure 7: Table for finding the value of C.....	25
Figure 8: Typical Overset Domain.....	27
Figure 9 Hull and Rudder Domains.....	28
Figure 10 Hull and Background Domain	29
Figure 11: Domain Size [shown for hull as reference].....	30
Figure 12: Domain Locations [Profile View].....	31
Figure 13: Uniform cell diffusion.....	31
Figure 14: Hull Domain [After Meshing]	32
Figure 15: Hull Domain Cut Plane [After Meshing].....	32
Figure 16: Refinement Sector near propulsion device	34
Figure 17 Flow refinement sector.....	34
Figure 18: Typical Y+ regions	35
Figure 19 Hull Domain reference with VL	36
Figure 20 Overlapping boundary refinement at free surface.....	37
Figure 21 Overlapping Domain.....	38
Figure 22: X Direction Drag Force [Acc]	41
Figure 23: Heave [Acc].....	42
Figure 24: Pitch [Acc].....	42
Figure 25: Actuator disk No 1 [Thrust].....	43
Figure 26: Actuator disk No 2 [Thrust and Torque].....	43
Figure 27: Free surface Elevation.....	44
Figure 28: Resultant Force [TC].....	44
Figure 29: Sway Motion [TC]	45
Figure 30: Heave Motion [TC].....	45
Figure 31: Roll [TC].....	46
Figure 32: Pitch [TC]	46
Figure 33: Yaw rate [TC].....	47
Figure 34: Mass Fraction [TC].....	47
Figure 35: Relative Velocity [TC].....	48
Figure 36: Free surface [TC]	48
Figure 37: Free surface [TC]	49
Figure 38: Vessel Trajectory [6 DoF Simulation].....	51
Figure 39: Vessel Trajectory [3 DoF Simulation].....	52
Figure 40: Residual becoming invalid.....	53

List of Tables

Table 1: Principal Particulars	2
Table 2: Summary of RESOLUTION MSC.137(76).....	4
Table 3 Limitation of Empirical Formula	6
Table 4 Standard Parameters and their meaning	7
Table 5: Domain size (brief)	29
Table 6 Value of Domain Size (Rudder).....	30
Table 7: Comparison between mesh.....	40
Table 8: Solved Parameter for 3 DOF and 6 DOF	49
Table 9: Computation Time	50
Table 10: Comparison for 3 DOF and 6 DOF	50
Table 11: Comparison for 3 DOF and Full-Scale Trial.....	50
Table 12: Comparison for 6 DOF and Full-Scale Trial.....	51

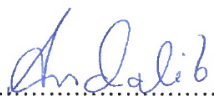
Declaration of Authorship

I, **Abu Afree ANDALIB**, declare that this thesis and the work presented in it are my own and have been generated by me as the result of my own original research. The title of my Masters' thesis is: **“Development of methodology for predicting marine vessel turning radius with overset grid technique using CFD Solver”**


I confirm that:

1. This thesis work has been carried out for the requirement of the research degree at the specified university.
2. I have acknowledged all main sources of help.
3. Where I have consulted the published work of others, it is always clearly attributed.
4. Where I have quoted from the work of others, the source is always given. With the exception of such quotations, this thesis is entirely my own work.
5. Where the thesis is based on work done by myself jointly with others, I have made clear exactly what was done by others and what I have contributed myself.
6. This thesis contains no material that has been submitted previously, in whole or in part, for the award of any other academic degree or diploma.
7. I cede copyright of the thesis in favour of Ecole Centrale de Nantes

Signed:


.....

Place and Date:


.....

Dedication

I would like to dedicate my thesis to my dearest parents who have given me all their blessings and efforts to ensure that I have this excellent opportunity and privilege of education. Their love, inspiration, encouragement and support kept me going through my difficult times.

Acknowledgement

I would like to express my deepest appreciation to all those who provided me the possibility to complete this report. A special gratitude I give to my supervisor, Nolwenn Huon De Kermadec, whose contribution in stimulating suggestions and encouragement, helped me to coordinate my project especially in writing this report.

Furthermore, I would also like to acknowledge with much appreciation the crucial role of the Company President and Chief Executive Officer Mr. Vincent Seguin, who gave the permission to use all required equipment and instructed with necessary directions to complete the thesis titled as “*Development of methodology for predicting marine vessel turning radius with overset grid technique using CFD Solver*”.

A special thanks goes to all my colleagues and the entire team of Mauric. They helped me and gave suggestion about the different issues faced throughout the internship and thesis period. Last but not least, I have to appreciate the guidance given by other senior colleagues especially in my project for their comment and advices.

I would also like to thank the entire team of FineMarine CFD Solver and specially Mr. Etienne from their support system to help me with all the software related issues.

Finally, I would like to express my gratitude to professor Mr. Philippe RIGO from University of Liege. I would also like to articulate my deepest appreciation to my academic advisor and EMSHIP program coordinator at Ecole Centrale de Nantes, professor Mr. Lionel GENTAZ. I will be forever grateful to my two professors for providing me with academic support and guidance as required. I would also like to take this opportunity to thank all the Professors from University of Liege and Ecole Centrale de Nantes for their patience and providing us with necessary knowledge required to complete this work. I would also like to thank all the people who have supported me to complete the research work directly or indirectly.

Abstract

Finding the turning radius of a ship at an early stage is an interest for both naval architects and the vessel operators. The intention is to predict the turning radius with a reasonable allowance. The most accurate with lowest error prediction at design stage is to conduct a scale model test but it is financially demanding. The development of computational method allows to conduct such multidomain calculations with allowable deviations from real result.

Many empirical, semi-empirical formulations are available for large displacement vessel with some limited value application but no formulation for high speed or medium speed vessel are not available. Most of the cases, high speed or medium speed vessels have model test results in order to determine the turning radius. In order determine this factor, researchers focus on finding the pressure variation and fluid interaction with hull at high speed. The rudder shape, size, flow at the stern, propeller side force, transverse hull moment was studied. Researchers also try to find coupled 6 DOF equation and inboard outboard roll angle. A couple of empirical formulation were found with very limited application and also the rudder and propeller force were calculated as average. The interaction between them were also not considered.

The aim of the study is to find the turning radius for these medium or high-speed vessel with overset grid technique using computational fluid dynamics. Overset grid is relatively more accurate when domains interact and need to transfer cell data between them as in the case of turning maneuvering. The thesis focuses on finding the appropriate physical behavior for high-speed vessel and combining that behavior on a CFD solver in order to predict turning radius as accurate as possible.

A 6 DOF coupled equation was considered as the real behavior is coupled with different DOFs. K omega SST model was used as turbulence model as $k - \omega$ model is used near the solid wall and $k - \epsilon$ model is used away from the wall by using a blending function. The model also considers the turbulent shear stress transport.

The research signifies on the accurate behavior of turning radius prediction using overset grid method. With an optimized mesh a 15.4 % close prediction was found using a bare hull without wave generator.

Keyword: Turning Radius, Maneuvering, Overset, CFD, K omega turbulence model, 6 DOF motion Equation

Chapter 1 Introduction

This Master's thesis and internship report is prepared as part of the internship conducted on the organization named, Mauric, a private company with a management board, registered under SIREN 331430306 and based in MARSEILLE (13001). The company specializes in the naval and maritime engineering sector along with technical studies. The internship was conducted as a requirement for the Masters of Science degree and was conducted after an agreement was formed among three parties, namely Ecole Centrale de Nantes, Mauric and the author himself. The internship is titled as, "**Development of methodology for predicting marine vessel turning radius with overset grid technique using CFD Solver**". The intention of the study is to find the Turning circle of a vessel and stopping distance of a vessel using computational fluid dynamics.

In order to model and understand the physics behind maneuvering of a high-speed vessel, an intensive study on the theoretical aspect was done at the beginning of the study. The reason was to find out the correct combination of meshing and theoretical models to incorporate in the computation algorithm.

The next sections are devoted to problem statement, formulation and Scope of the report. The highlighted parts are visible in *Italic* and the Section headings of each chapter are visible in **Bold**. The thesis is written with standard spacing, formatting and font size as guided by the advisory board of University of Liege and Ecole Centrale de Nantes. The citation of the source reference in the last chapter are in APA (American Psychological Association) or/and MLA (Modern Language Association) guideline where possible. The referencing for only research paper inside the thesis is done using APA format.

1.1 Problem Statement and Motivation

The prediction methodology of turning circle for a high vessel can still be considered as under developed. There is a well-established methodology for displacement vessels with moderate speed and it can be well predicted using CFD and analytical method within a considerable accuracy. It is obvious that the actual behavior of the ship is much complicated due to numerous factors playing at the time of turning. For high-speed vessels, as they are prone to pitch up and heave during their operation. The real behavior is much complicated and required extensive modelist approach. However, this will also not be able to predict the exact turning circle distance due to the factors related to that environment. *The intention is then shifted to prediction of the turning circle as close to actual value as possible with minimum costing for meshing using computational fluid dynamics.*

The following picture shows a general turning circle diagram depicting different terms identified throughout the operation. *While all of them are important for the operation of the vessel in the open and restricted waterways, the author and the naval architects are mostly interested in finding the Tactical Diameter of the vessel. The Tactical diameter can be*

addressed as the distance between initial approach line and the 180-degree approach line in parallel with the initial approach line.

1.2 Formulation

The theoretical study was sub divided into hull behavior, rudder behavior and propeller behavior. *A monohull with a hard chine but with no bow thruster and no extra appendage is taken as reference. It is obvious that hull with bow thruster, appendage and multiple hulls will experience a different flow dynamics and hence the turning circle behavior will be different. It requires designer's decision in case of efficient meshing and CFD modelling.*

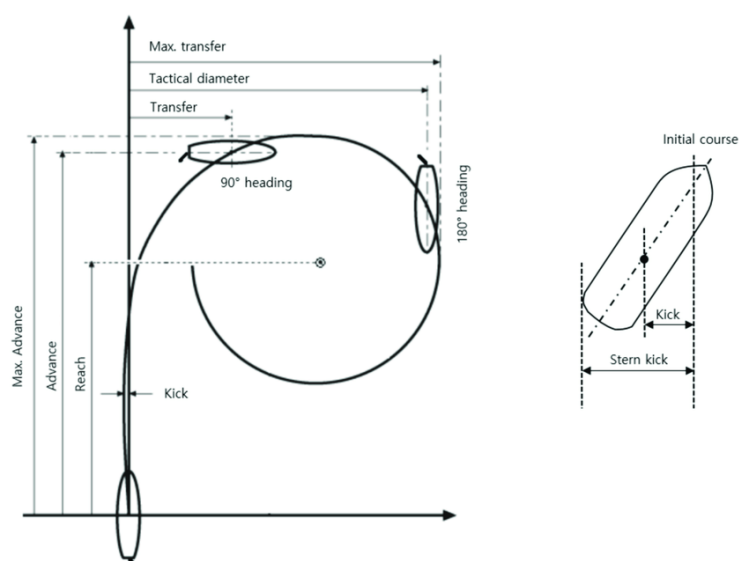


Figure 1: A universal turning circle diagram

[Image and Diagram Source: (Kim, 2020) [\[1\]](#)]

A reference vessel was selected for the simulation purpose with permission to the company authority and the availability of full-scale test was ensured. The vessel principal particulars are listed on the table below:

Table 1: Principal Particulars

Principle Particulars	Unit [m]
LOA	60.77
Breadth	9.55
Depth	7.62

1.3 Objective of the thesis

The objectives of this thesis are listed below:

- To develop a methodology for calculation of turning radius and stopping distance using overset grid technique of a marine vessel.
- Validation of the simulation results using test data.

1.4 Scope of the thesis

The report is constructed in four chapters including introduction.

Chapter 2 is titled as “**Literature**”. It has sections dedicated to regulations, basic equation of motion, hull, rudder, propeller behavior. The chapter also contains further extensive works including multiple hulls, appendages etc.

Chapter 3 is titled as “**Methodology, Simulation and Validation**”. It has sections dedicated to mesh generation, flow solver and obtained results. The chapter also contains further extensive works including Stopping distance calculation. The software used in this case was FineMarine 10.1. ***Some graphs are presented without axis data in order to maintain confidentiality.***

Chapter 4, titled as “**Conclusion and Recommendation**”, provides a summary, limitations of the report and discuss about further working scope along with recommendations to proceed.

Chapter 5, titled as “**Reference**”, provides the segregated citation for the theoretical bibliographies used in the report.

Chapter 2 Literature

In this chapter, the detailed theoretical finding will be presented in different sections dedicated to the different equipment of the vessel. The first task was to study the regulatory guidelines in order to have a complete idea of the behavior of the vessel during maneuvering. The theoretical research papers, books, lecture notes and published master's thesis was studied after that. All the citation are mentioned in the “**Reference**” section. The intention was to find out the relevant information related to the vessel maneuvering and summarize them to understand the required works to be carried out. The sequence mentioned in this chapter was followed to have a complete understanding of the subject matter from developing the physics to find the correct mesh and turbulence model combination to capture the phenomenon.

2.1 IMO, ITTC and Rulebooks

The International Maritime Organization (IMO) is the primary regulatory body of maritime operations and its task is to promote safe, secure, environmentally sound, efficient and sustainable shipping through cooperation. It publishes and regulates guidelines related to maritime affairs. The organization focus on different aspects of global acquisition of safe marine transport and one of them is Maritime Safety Committee. It deals with matters related to maritime safety and security that are under IMO and it covers both passenger ships and all types of cargo vessels. The committee publishes resolution which are the final report of the committee meeting when they were adopted. For vessel maneuvering, the document is titled as “STANDARDS FOR SHIP MANOEUVERABILITY” ^[2] with the report number being “RESOLUTION MSC.137(76)”. It means the standards were finalized in report number 137 of 76th session of Maritime Safety Committee (MSC). The findings from the document are summarized below:

Table 2: Summary of RESOLUTION MSC.137(76)

IMO – Maritime Safety Committee (MSC) 137(76) Important Parameters		
Criteria Type	Parameter	Remarks
General	Speed	The vessel should be travelling at 90% of its operating speed at 85% Maximum Continuous Rating (MCR)
	Approach Type	Steady with Zero yaw angle
	Rudder angle	Maximum permissible rudder angle or 35 degrees
	Loading condition	Full Load (summer load line) and even keel
	Environment	Deep, unrestricted water with as calm environment as possible
	Length, L	Specified as Length between perpendiculars
Specified	Advance	Should be less than 4.5 L
	Tactical Diameter	Should be less than 5 L
	Track reach for stop	Should be less than 15 L

The International Towing Tank Committee (ITTC) is an association responsible for prediction of various hydrodynamic parameters based on the physical and numerical experiments. The organization also provide guidelines and methodologies for conducting sea trials and

experiments to determine different parameters. A number of ITTC documents were studied in order to find the correct relation between conducting the simulation while still maintaining an experimental validity. The ITTC document titled "Testing and Extrapolation methods maneuverability free running model tests" [3], with document number being 7.5-02-06-01 states the complete procedure for conducting the test in scale models with different control system and also discuss the process to data acquisition. The document states that depending on the basin size model should be chosen as large as possible in order to reduce the scale effect. Propeller thrust, inertia matrix and roll angle should be defined earlier while still maintaining a deep-water condition. The document also suggests to avoid tank wall interference and correct Froude scaling to have a more realistic boundary layer. Based on that the computational modeling for the domains on the software were developed. The vessel that was used for computing was in full scale but if it is not possible to a full-scale computation due to less core or expense a scale model can also be used. The complete procedure for domain creation with avoiding all these warnings are discussed in [Chapter 3](#).

The ITTC document titled "Full Scale Maneuvering Trials", [4] with document number being 7.5-04-02-01 states the procedure for conducting the test in full scale with different control system and also discuss the process to data acquisition. The document discusses a lot of acceptance test in maneuvering along with turning circle for example pullout test, parallel course keeping test, man overboard test etc. but the intention for this case is to focus only on the turning circle test. The document states to determine the maximum sea state on the test area based on IMO regulations. The guideline also suggests to find out velocity loss, rate of turn etc. To keep those criteria same in the case, the vessel to be modelled for simulation was checked for the location and sea state of test location which was found to be at sea state 2 with peak period of 7.5 seconds and wave height of 0.3 m.

The ITTC document titled "Evaluation and Documentation of HSMV" [5] with document number being 7.5-02-05-05 states the identification of high-speed vessels based on the Froude number. According to 1996 session of 21st ITTC which refer to the IMO (2008) Code of Safety of high-speed craft, the vessel should qualify the following criteria while maintain a speed of more than or equal to 25 knots:

$$Fr_{\nabla} = \frac{V}{\sqrt{g \cdot \nabla^3}} > 1.18$$

Equation 1

The ITTC document titled "Validation of Maneuvering simulation models" [6] with document number being 7.5-02-06-03 states the validation procedure for generic maneuvering prediction methods. In general, the loading condition has to be maintained as same as the actual vessel. This means, the KG, design draft and design displacement are to be ensured along with other parameters. Apart from this, the engine power, propulsor parameters and steering devices are to be maintained as the actual vessel. The document also mentions about the captive model test procedures but that is not the requirement for now. In regard to the instructions, the actual loading conditions was maintained with the value of KG and other parameters. An actuator disk was positioned at the same location of the propulsor as per design. Inertia matrix was also calculated and was set up as an ideal dynamic parameter.

The ITTC document titled "Guideline on the use of RANS tools for maneuvering prediction" [7] with document number being 7.5-03-04-01 states the computational modelling procedure for

generic maneuvering simulation methods. The guideline suggests to solve the relevant partial differential equations (PDE) with the help of Finite Volume Method (FVM) and also with appropriate turbulence model. During fluid flow modelling, propeller slip, propeller swirl and rudder stall angles has to be checked simultaneously as they can have a varied effect. RPM variation with torque has to be kept in mind while maintaining a stable performance from the propulsor devices. Despite the need of having a lot of computational power, sliding grids and overlapping grid is highly recommended to model the propeller turning and deflection of rudder. The document suggests a typical dimension for the domain with about 3-5 times of ship length in longitudinal directions and 2-3 times in transverse directions. Near wall mesh has to be implied correctly in order to correctly insert the viscous layer and capture the flow near the boundary region. Designer's judgement is required when modeling sinkage and trim as they can induce large drift angle or yaw rate. In that aspect, the vessel chosen for analysis was modelled with adequate domain size based on the guidance from ITTC and the CFD Solver authority. The propulsion was modeled with actuator disk rather than having a physical propeller on the disk which could be more computationally demanding.

The classification society rulebooks also state their own regulations, in some cases with empirical formulation with limited application are also given. These are based on the full-scale trial results and the regulation provided by parent regulatory body such as IMO. The guideline for vessel maneuverability published by ABS (American Bureau of Shipping) [8] has some formulations to the documents. However, they are limited to the application based on different parameters. Some of them are mentioned in the table below.

Table 3 Limitation of Empirical Formula

Application to Single Screw Monohull only		
Parameter	Minimum	Maximum
Length [m]	55	350
C_b	0.56	0.88
Rudder Angle, δ_R [deg]	10	45
$\frac{L}{B}$	5.56	9.91
$\frac{V}{\sqrt{L}}$ [knot/m ^{0.5}]	0.20	1.0

[Source: ABS Vessel Maneuverability Guideline, Appendix 4, Table 1 [8]]

If the vessel parameters are within these values, the steady turning diameter can be calculated from the following equation.

$$\frac{STD}{L} = 4.19 - 203 \left(\frac{C_b}{\delta_R} \right) + 47.4 \left(\frac{Trim}{L} \right) - 13 \left(\frac{B}{L} \right) + \left(\frac{194}{\delta_R} \right) - 35.8 \left(\frac{S_p}{L} \right) \cdot \left(\frac{Ch}{T} \right) \cdot (ST - 1) + 3.82 \left(\frac{S_p}{L} \right) \cdot \left(\frac{Ch}{T} \right) \cdot (ST - 2) + 7.79 \left(\frac{A_B}{L.T} \right) + 0.7 \left(\left(\frac{T}{T_L} \right) - 1 \right) \left(\frac{\delta_R}{|\delta_R|} \right) \cdot (ST - 1)$$

Equation 2

[Source: ABS Vessel Maneuverability Guideline, Appendix 4 [8]]

The next is to calculate the tactical diameter and advance based on the ship length.

$$\frac{TD}{L} = .910 \frac{STD}{L} + .424 \frac{V_s}{\sqrt{L}} + .675$$

Equation 3

[Source: ABS Vessel Maneuverability Guideline, Appendix 4 [81]]

$$\frac{Ad}{L} = .519 \frac{TD}{L} + 1.33$$

Equation 4

[Source: ABS Vessel Maneuverability Guideline, Appendix 4 [81]]

All of these parameters mentioned in the equation are stated on the table below with their usual meaning.

Table 4 Standard Parameters and their meaning

Parameters used in the above equations		
Parameter	Meaning	Unit
STD	Steady turning diameter	Meter
C _b	Block coefficient	-
δ _R	Rudder Angle	Degree
Trim	Static Trim	Meter
L	Length between perpendiculars	Meter
B	Molded breadth	Meter
S _p	Rudder span	Meter
Ch	Mean chord length of rudder	Meter
T	Design draft at full load	Meter
ST	Stern type [1 = Closed and 2 = Open]	-
T _L	Estimated draft at Turning Circle	Meter
A _B	Bow profile area	Meter ²
TD	Tactical Diameter	Meter
V _s	Test Speed	Knots
Ad	Advance	Meter

[Source: ABS Vessel Maneuverability Guideline, Appendix 4 [81]]

2.2 Equation of Motion

The prediction of maneuverability is basically solving the Newtons second law of motion with acceleration being in its second derivative form. Integrating the equation will show position along with time which is basically a maneuvering motion.

$$F = m \frac{d^2x}{dt^2}$$

Equation 5

Here the force, F can be taken as only the hull generating force for simplicity. It can also be taken as a combination of hull, rudder, propeller, environmental and incident wave force. The hull force generally induced due to the turning moment generated by the rudder. The hull

counteracts by generating a moment as well which induces all the hull force. The direction of the vessel depends on the net hydrodynamic moment. The rudder and propeller can act as one single unit in order to generate a turning moment (Azipod, as example).

The behavior can be seen in the figure below shows the rudder angle deflection with a counter moment generated in the opposite direction. The rudder aligns to the port side creating a drift angle and a moment M_{Tz} is created in the opposite direction. The hull will turn eventually to port as the net hydrodynamic moment is opposite of M_{Tz} .

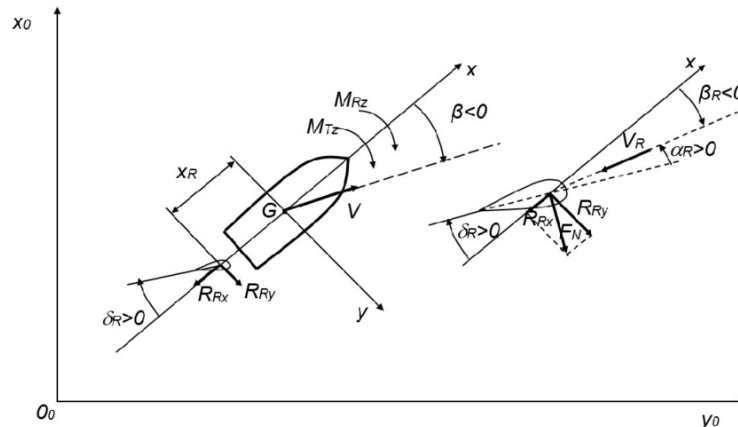


Figure 2: Moments and Rudder interaction in turning

[Image and Diagram Source: (Tadeusz, 2018) [9]]

Bowles (Bowles, 2012) [10] identified and examined high speed monohull craft for their typical behavior and maneuvering performance in various parameters. Turning circle assessment was one of them. It was concluded and remarked that vessel with hard chine can be leading to different response and the dynamic effects during high-speed maneuvering are significant as the motion and acceleration is strongly coupled in all the axes. The behavior depends on the vessel hull form, transverse stability, position of the appendage and rudder type with execution time. The loss of speed and the change is yaw or inducing a drift angle is apparent. The author balanced the equation of motion with consideration of particle experiencing transverse force and centripetal force. These forces are balanced until the new equilibrium state is reached. Since the vessel is now experiencing a different flow at the bow, it induces drag and slow the vessel down. The author referred to (Sugai, 1963) and (Martin, 1976) concluding that high speed vessels tactical diameter tends to increase with speed and the rate of turn decreases.

Lewandowski (Lewandowski, 2004) [11] mentioned different parameters responsible for maneuvering in the equation of motion. It was suggested that added mass have a high impact on the high-speed configuration and the coefficient can be calculated using a numerical software with potential flow theory. For a complicated geometry with appendage, in order to reduce computation effort, the coefficient for these appendages can be calculated separately to be accounted in the equation of motion. The author stated that the steady hull force is primarily hydrodynamic drag and pressure induced force whereas the rudder force is primarily viscous force. It was found that having higher order terms in the equation does not necessarily mean having more accurate result. The motion equation can get very complicated with the inclusion of high order terms, coupling of terms and the number of DOFs to be solved. A simple set of maneuvering equations are given in the SNAME workbook of maneuverability. This

formulation has some empirical coefficient that can be extracted from the SNAME guideline. In the equation, U is the approach speed, v is the sway velocity and r are the yaw rate. X, Y and N define the surge force, sway force and yaw moment respectively.

$$\begin{aligned} X_s &= a_0 + a_3v^2 + a_7r^2 + a_9vr \\ Y_s &= b_1Uv + b_3Ur + b_{13}|v|r + b_{15}vr^2 + b_{26}|v|v + b_{28}|r|r \\ N_s &= f_1Uv + f_3Ur + f_{13}|v|r + f_{15}vr^2 + f_{26}|v|v + f_{28}|r|r \end{aligned}$$

Equation 6

For high-speed configuration these equations are not enough as vertical motion and trim change are highly significant. All the hydrodynamics coefficient are strongly dependent on the speed of the vessel. Since the vessel experience vertical motion and trim change, the underwater geometry is changed. As a result, it effects the longitudinal and vertical and lateral forces which results in coupling of the motion. Flow velocity around the hull will be different from point to point even though steady condition is assumed. Vorticity shed from the transom and interaction with appendage, rudder will also create a complicated motion behavior. If a linear model is used, the linear coefficients can be found model test in order to develop the mathematical model. The author considered high speed for a range of Froude number between 0.7 – 0.8. With consideration of linear terms only, the surge, sway, roll and yaw motion equation can be written as following respectively and it is developed for hard chine vessels:

$$\begin{aligned} X_s &= m\dot{u} \\ Y_s &= Y_{\dot{v}}\dot{v} + Y_vv + Y_{\dot{\phi}}\dot{\phi} + Y_{\phi}\ddot{\phi} + Y_{\phi}\dot{\phi} + Y_{\dot{\psi}}\dot{\psi} + Y_{\psi}\ddot{\psi} \\ K_s &= K_{\dot{v}}\dot{v} + K_vv + K_{\dot{\phi}}\dot{\phi} + K_{\phi}\ddot{\phi} + K_{\phi}\dot{\phi} + K_{\dot{\psi}}\dot{\psi} + K_{\psi}\ddot{\psi} \\ N_s &= N_{\dot{v}}\dot{v} + N_vv + N_{\dot{\phi}}\dot{\phi} + N_{\phi}\ddot{\phi} + N_{\phi}\dot{\phi} + N_{\dot{\psi}}\dot{\psi} + N_{\psi}\ddot{\psi} \end{aligned}$$

Equation 7

The hydrodynamic coefficient can be found using a model test or using an empirical formulation. A list of empirical formulations is also given by the author.

Zhang et al. (Zhang, 2017) [\[12\]](#) adopted a hybrid coordination system to define the motion and used the MMG model for the research. Inclusion of second order regular wave is able to make the result much closer to the experimental values. The author separated forces in the maneuvering motion equation in segment of hull, rudder, propeller and wave. In the equation m is ship's mass while I_{zz} is moment of inertia about z axis and x_G represents the x-coordinate of the center of gravity and m_x , m_y and J_{zz} are the corresponding added masses and added moment of inertia.

$$\begin{aligned} (m + m_x)\dot{u} - (m + m_y)vr - mr^2x_G &= X_H + X_P + X_R + X_W \\ (m + m_y)\dot{v} + (m + m_x)ur + m\dot{r}x_G &= Y_H + Y_R + Y_W \\ (I_{zz} + J_{zz} + mx_G^2)\dot{r} + m(\dot{v} + ur)x_G &= N_H + N_R + N_W \end{aligned}$$

Equation 8

Faltinsen (Faltinsen, 2005) [\[13\]](#) developed a set of linear equations for deep water at high and moderate Froude numbers. The application was done while keeping in mind about directional stability, steady state turning and also for multihull vessels. The author also discussed about the nonlinear viscous effect in deep water condition as well as the possibility of coupling of the respective motions.

The author assumed a body fixed coordinate system along with linear sway and yaw motion. These two motions are defined by η_2 and η_6 . The 2D horizontal force on the hull is represented by the following equation with a_{22} being the added mass coefficient:

$$f_2^{HD} = - \left(\frac{\partial}{\partial x} + U \frac{\partial}{\partial x} \right) [a_{22}(\eta_2 + x\eta_6)]$$

Equation 9

The motion equation in steady state was balanced by the hydrodynamic forces created by hull and rudder with the complete centrifugal force. In case of multi hull interaction, it is suggested to determine the hull-to-hull interaction and include that in the motion equation.

$$\frac{MU^2}{R} = Y_v v + Y_r r + Y_\delta \delta$$

Equation 10

The transverse hull force is $(Y_v v + Y_r r)$ and the rudder force is $Y_\delta \delta$

In case of Nonlinearity, the interaction of yaw and sway velocities can result in nonlinear viscous effect. Cross flow principle can be used to determine viscous transverse drag force and is valid in low-speed maneuvering because it is based on the assumption that transverse velocity component is larger than the forward component. It assumes flow separation due to a cross flow past the ship.

To find the more accurate drag coefficient, and to have free surface effect, bilge effect, beam to draft ratio and turbulence, 2D + t [\[14\]](#) principle can be applied when the forward speed is relatively high compared to the transverse velocity component. Turbulent boundary flow will change the separation point and thus has a strong influence on the drag coefficient.

With that consideration in mind, it was decided to investigate the cross flow drag induced at the vessel in order to under the physical phenomenon more accurately. This will allow the user to understand what will be the dominant term in case of drag calculation. If possible, there is also a scope to work on the source code so that the more dominant parameter can be exploited as most commercial software codes are written on a specific direction.

Hooft (Hooft, 1994) [\[15\]](#) investigate the cross flow drag induced on a ship specifically on maneuvering motion. The attention was given to the longitudinal distribution of the nonlinear components of the lateral force. It was believed that this component will have a more dominant action when the vessel is taking a tight turn. The author stated that captive model tests are not always perfect when comparing the hydrodynamic coefficients of two vessels. Also, the simulation accuracy will be highly dependent on the accuracy of these coefficients. Some empirical formulations were presented as a function of the principal particulars of the vessel by Kijima et al. (Kijima, 1990) [\[16\]](#). The reason for their accuracy is predicting the correct linear

hydrodynamic coefficient near the bow or stern of the vessel. This is highly depended on the cross flow and flow separation at these areas. The author considered lateral hydrodynamic force on the vessel is a reaction to ships drift velocity v at zero rate of turning. In non-dimensional form the lateral force will be as the following equation with β being the drift angle.

$$Y(\beta)' = Y_{\beta}' \cos(\beta) \sin(\beta) + Y_{\beta\beta}' \sin\beta |\sin\beta|$$

Equation 11

The equation can be rewritten as the following

$$Y(\beta)' = Cy_n \cos(\beta) \sin(\beta) - Cd_n \sin\beta |\sin\beta|$$

Equation 12

The Cy_n can be written as the following equation form which will give the drag coefficient equation.

$$Cy_n = Cl_{\beta} \cos(\beta)$$

Equation 13

$$Cd_n = \frac{Y(\beta)' - Cl_{\beta} \cos^2(\beta) \sin(\beta)}{\sin\beta |\sin\beta|}$$

Equation 14

The lift can be determined as a function of local lateral added mass along a distance ξ and added mass of water per unit length, m_y .

$$L = uv \int_{\xi_a}^{\xi_f} m_{y\xi} d\xi$$

Equation 15

With the local lift coefficient, Cl_{β} determined on the parts, it is now possible to determine the cross-flow coefficient, Cd_n . Even though the maneuvering is assumed to be steady but a maneuvering ship will experience a drift angle while making the turn, the cross-flow coefficient can be predicted by means of empirical formulation. In theory it should be good enough to predict the drag and cross flow separation. Since RANSE solver will be used and viscous equation will be solved, the drag force will be obtained otherwise.

The attention then shifted to the finding the roll motion factor in case of maneuvering. As stated earlier for high-speed vessels the rolling motion is quite significant, it was decided to investigate the rolling motion. The rolling motion can be coupled, non-coupled, linear, nonlinear or any sort of combination.

Cao (Cao, 2017) [\[17\]](#) investigated the roll motion of a high-speed monohull and tried to predict the roll motion using a genetic algorithm. A scale model prototype was developed with a complete set up with experimental capability. Three mathematical models were compared with combination of linear and nonlinear actions. The first model considers the damping angle and restoring moment as linear. The second model considers the damping angle as nonlinear and

restoring moment as linear. The third model considers the damping angle and restoring moment as nonlinear. They are shown below respectively

$$\ddot{\varphi} + \frac{2N_{\theta}}{I_x} + \frac{Dh}{I_x} \sin\varphi = 0$$

Equation 16

$$\ddot{\varphi} + 2 \left| \frac{N_{\theta}}{I_x} \dot{\varphi} + \frac{W}{I_x} \right| \dot{\varphi} |\dot{\varphi}| + \frac{x}{I_x} \dot{\varphi}^3 + \frac{Dh}{I_x} \sin\varphi = 0$$

Equation 17

$$\ddot{\varphi} + 2 \left| \frac{N_{\theta}}{I_x} \dot{\varphi} + \frac{W}{I_x} \right| \dot{\varphi} |\dot{\varphi}| + \frac{x}{I_x} \dot{\varphi}^3 + \frac{C_1}{I_x} \varphi^3 + \frac{C_2}{I_x} \varphi^2 + \frac{C_3}{I_x} \varphi = 0$$

Equation 18

Here, h is the high initial stability value, D is the displacement, φ is the roll angle, N_{θ} is the roll type damping coefficient, C_1 and C_2 are nonlinear coefficient and C_3 is linear coefficient. The researcher compared the values for the prototype with an acceptable error range.

Taylan (Taylan, 1996) [18] developed nonlinear roll equation of motion. Taylan (Taylan, 2004) [19] investigated the effect of forward speed of on vessel rolling. The investigation was done with a mathematical model and beam waves approaching to the vessel. The author concluded that at lower speed and lower Froude number (less than 0.25) the periodic roll resonance amplitude decreases and improve ship roll motion. As a result, at higher speed, it needs to be taken with caution. The nonlinear motion equation after splitting the damping moment into linear and nonlinear components and after replacing the coefficients with their respective expressions is shown below. The term m_L and m_N is linear and nonlinear damping coefficient respectively.

$$\ddot{\varphi} + m_L \dot{\varphi} + m_N \dot{\varphi} |\dot{\varphi}| + \omega_{\varphi}^2 \varphi + r_3 \varphi^3 + r_5 \varphi^5 = \lambda \omega_e^2 \alpha_m \cos \omega_e t$$

Equation 19

Hazuro (Hazuro, 1980) [20] developed roll motion equation and investigated for high-speed vessels. The author concluded that roll angle introduce asymmetry of understand portion of hull form relative to longitudinal centerline. It generated a yaw moment. For high-speed vessel, generally having small GM can introduce severe rolling motion.

Yang et al. (Yang, 2014) [21] conducted roll decay test on an unmanned vessel with eight kinds of mathematical model in order to validate the models. With each models the roll angle for initial condition was changed and it was found that righting moment did not change during the change of roll angle and it was linear.

Bikdash et al. (Bikdash, 1994) [22] investigated the influence of different damping models on the nonlinear roll dynamics with Milnikov analysis. The roll damping depends on many factors such as vessel speed, underwater profile, antiroll fins and bilge keels. The author concluded that linear plus cubic damping model shows good approximation for roll decay. In that context, it can be said that since high-speed vessels might need to have these appendages for decaying the roll at high speed.

The conclusion for hull force can be drawn at this stage. It is found based on the theoretical studies that for a bare hull, the cross flow can be an important factor for drag and flow separation aspect. The roll motion is also an important factor defining the complete behavior of the vessel. The intention now shifted to find out the rudder induced turning moments and forces.

Yasukawa et al. (Yasukawa, 2021) [23] investigated the rudder force on a vessel with drift angle in maneuvering condition. The author used the MMG model which is another model to predict and mathematically model the vessel motion in a turning. The author proposed the following set of equations respectively for surge, sway force and yaw moment for calculating and an initial estimate of the rudder force. In the following equations, F_N is the rudder normal force, δ is the drift angle and resistance deduction factor t_r , rudder force increase factor α_H , acting point of rudder force increase x_H and x_R is the longitudinal center of rudder usually 0.5 times length. Yoshimura et al. (Yoshimura, 2012) [24] also found the same equations as the previous author.

$$\begin{aligned} X_R &= -(1 - t_r)F_N \sin\delta \\ Y_R &= -(1 + \alpha_H)F_N \cos\delta \\ N_R &= -(x_R + \alpha_H x_H)F_N \cos\delta \end{aligned}$$

Equation 20

The author concluded about the rudder force, inflow velocity and drift angle. With drift angle more than 45 degree the inflow velocity maximum value. Since the original MMG model cannot capture this behavior, some modifications were proposed.

Delefortrie et al. (Delefortrie, 2021) [25] developed a mathematical model to find out the rudder force and torque on a vessel in maneuvering condition. The paper stated the rudder forces in X and Y direction as well as torque in the following set of equations. C_p defines the center of pressure.

$$\begin{aligned} F_X &= \frac{1}{2} \rho A_R v_R |C_L \sin\beta_R + C_D \cos\beta_R| \\ F_Y &= \frac{1}{2} \rho A_R v_R |-C_D \sin\beta_R + C_L \cos\beta_R| \\ F_Q &= \frac{1}{2} C_p \rho A_R v_R^2 |-C_D \sin\beta_R + C_L \cos\beta_R| \end{aligned}$$

Equation 21

Abramowski (Abramowski, 2005) [26] proposed a method to calculate propeller force during maneuvering. The author employed artificial intelligence for performance assessment of propeller in different configuration. The side force of the propeller, Y is given by the following equation where D is the diameter, n is the rpm, J is advance coefficient and K_Q is torque coefficient.

$$Y = 2\rho n D^3 V_y K_Q J$$

Equation 22

The author found the prediction using artificial intelligence shows a good agreement with propeller force prediction. They also show good agreement with the wake field assessed by RANS solver.

Dai et al. (Dai, 2021) [27], Moreno et al. (Moreno, 2011) [28] and Oldfield et al. (Oldfield, 2015) [29] performed experiments and compare the result obtained with numerical methods. The two endmost researchers conducted full scale trial for their vessel. The first researcher followed a 3 DOF equation developed by MMG. The specific vessel in this case is a SWATH. As a result, an extra parameter, hull to hull interaction was required. A scale model prototype SWATH was developed for the experimental purpose. The researcher achieved a maximum of 11.33 % error for a tactical diameter with a Froude number of .202. The second researcher conducted a full-scale trial of the vessel and found good agreement with the regulations. The endmost researcher tried to find the hydrodynamic coefficient with CFD solver. The author found good agreement with the result. In the simulation, spatial discretization error was found but it was quite small in magnitude.

In order to cross check, the rolling period and encountering frequency, a more rigorous approach was taken and further studies were conducted. Since it will be eventually required to validate and check with the full-scale test trial data. Bhattacharyya (Bhattacharyya, 1978) [30] proposed more simplified and generalized equation for these two parameters.

$$\omega_{\phi}^2 = \frac{\Delta GM_T}{I_{xx}'}$$

Equation 23

$$T = \frac{2\pi}{\omega_{\phi}} = 2\pi \left(\sqrt{\frac{\Delta GM_T}{I_{xx}'}} \right)^{-1}$$

Equation 24

Schoop-Zipfel (Schoop-Zipfel, 2016) [31] conducted numerical simulation and showed two different approaches to simulate the behavior of the vessel in waves during maneuvering. It was found from the research that two models are developed so far in order to simulate this type of phenomenon. The first one is a two-time scale model where motion can be divided into seakeeping and maneuvering motion and solving them separately. The other one is a unified theory where both motions are unified with one set of equations.

In case of two-time scale model, the author suggested that the equation can be written as sum of low frequency maneuvering motion and wave frequency seakeeping motion and it follows the linear superimposition. The author suggested a motion equation for seakeeping in the frequency domain and used the MMG notation for maneuvering motion. In the equation, f_e is the wave excitation load for irregular waves.

$$M\dot{v} = -A(\omega)\ddot{\xi} - B(\omega)\dot{\xi} - C\xi + f_e$$

Equation 25

In case of unified theory, the system provides a direct coupling of low frequency maneuvering motion and the wave frequency motion. The maneuvering motion is followed by the first order wave loads. The equation is seen as the following:

$$M\dot{v} = -A(\alpha)\dot{v} - Dv - \int_{-\alpha}^t k(t-\tau)[v(\tau) - Ue_1]d\tau - C\eta + f_e$$

Equation 26

In the above equation, v is the body fixed velocity, $A(\alpha)$ is hydrodynamic coefficient, D is the damping term. The author found that both of these methods are significant enough to capture the behavior but there are room for improvement. The author preferred the unified theory since it can be done with only one set of equations.

Mucha (Mucha, 2017) [32] also considered the maneuvering motion and considered hull, rudder and propeller force to be treated separately. In case of the rudder force, the author suggested to consider the inflow velocity towards the rudder, v_R . It was found that the propeller slipstream effects the rudder inflow and increase the effective wash on the rudder surface. The local velocity or in generic the rudder velocity can be taken as the following equation:

$$V_{Rudder} = u(1-w)\sqrt{1+C_{th}}$$

Equation 27

Here C_{th} is the thrust load coefficient and w is the nominal wake fraction number. The propeller force is also suggested to take after the thrust deduction factor by the author. Considering all of these, the author suggested a set of linear equations for motion and straight-line stability analysis. The set of equation is mentioned below:

$$\begin{aligned} M\dot{x} + Nx &= F_r \delta \\ M &= \begin{bmatrix} -Y_{\dot{v}} + m & -Y_{\dot{r}} + mx_g \\ -N_{\dot{v}} + mx_g & -N_{\dot{r}} + I_z \end{bmatrix} \\ N &= \begin{bmatrix} -Y_v & -Y_r + mU_0 \\ -N_v & -N_r + mx_g U_0 \end{bmatrix} \\ x &= [v \ r]^T \\ F_r &= [Y_{\delta} \ N_{\delta}]^T \end{aligned}$$

Equation 28

Here M is the mass and inertia matrix and N is the damping matrix.

Matusiak et al. (Matusiak, 2012) [33] introduced the ship motion equation in a stern quartering sea with wave system modelled imbedded. The equation shows all 6DoF in time domain. In this case only surge force and sway force are shown.

$$\begin{aligned} &(m + a_{11})\dot{u} + a_{15}\dot{q} \\ &= -mg\sin\theta + X_{resistance} + X_{Propeller} + X_{Rudder} + X_{Wave} + X_{Maneuvering} - k_{15} \\ &+ (m + a_{22})(rv - qw) \\ &(m + a_{22})\dot{v} + a_{24}\dot{p} + a_{26}\dot{r} \\ &= mg\cos\theta\sin\varphi + (m + a_{11})(pw - ru) + Y_{Rudder} + Y_{Wave} + Y_{Maneuvering} - k_{22} \\ &- k_{24} - k_{26} \end{aligned}$$

Equation 29

Khanfir et al. (Khanfir, 2011) [34] introduced a procedure to determine the hull rudder interaction coefficient during maneuvering for single propeller single rudder (SPSR) and single propeller twin rudder (SPTR) configuration. The general procedure is to run a captive model test (CMT) in order to determine the “Flow straightening coefficient of sway velocity for port and starboard rudder”.

Park et al. (Park, 2021) [35] conducted performance prediction for a twisted rudder. However, this is not directly linked to the maneuvering motion or problem discussed hereby. But the findings are quite inquisitive. It was concluded that the total lift force slope of each twisted rudder was similar to each other and slightly greater than the flat rudder. It indicates that the twisted rudder may be a better option for maneuvering performance than any type of flat rudder.

Katayama et al. (Katayama, 2009) [36] developed a method for maneuvering simulation of high-speed craft specifically. In this case the author used the hydrodynamic forces obtained by model tests. The vessel taken as test bed in this case was a trimaran. The position of the side hull can have a change in the turning circle behavior. The sides hulls moving ahead will make the turning circle smaller due to increased yaw angular velocity.

2.3 Proposed Numerical Model

At this section, the mathematical model for all 6 DoFs will be stated. The coordinate system has to be defined at the beginning. The equations studied were found to be both linearized and sometimes nonlinearized. The moment or force coupling for some cases were observed. It is to be stated that the actual motion for a high vessel or medium speed vessel is nonlinear and coupled motion as there are numerous factors present while the maneuvering motion is conducted in full scale. Researcher try to simplify the model since computing all those factors or parameters are computationally demanding.

2.3.1 *Coordinate System and initial equation set*

The coordinate system that will be followed for the simulation as well as the theoretical studies is the body fix coordinate system rather than an earth fixed coordinate system. The earth fixed coordinate system is defined by the three dimensions and is related to the observer located on the earth surface. All the bodies can be tracked based on the observer’s location using the coordinate system.

Body fixed coordinate system is when the observer is positioned on the body itself and consider that as the base reference point. The three dimensions in this case is based on the position of the observer located on the body itself.

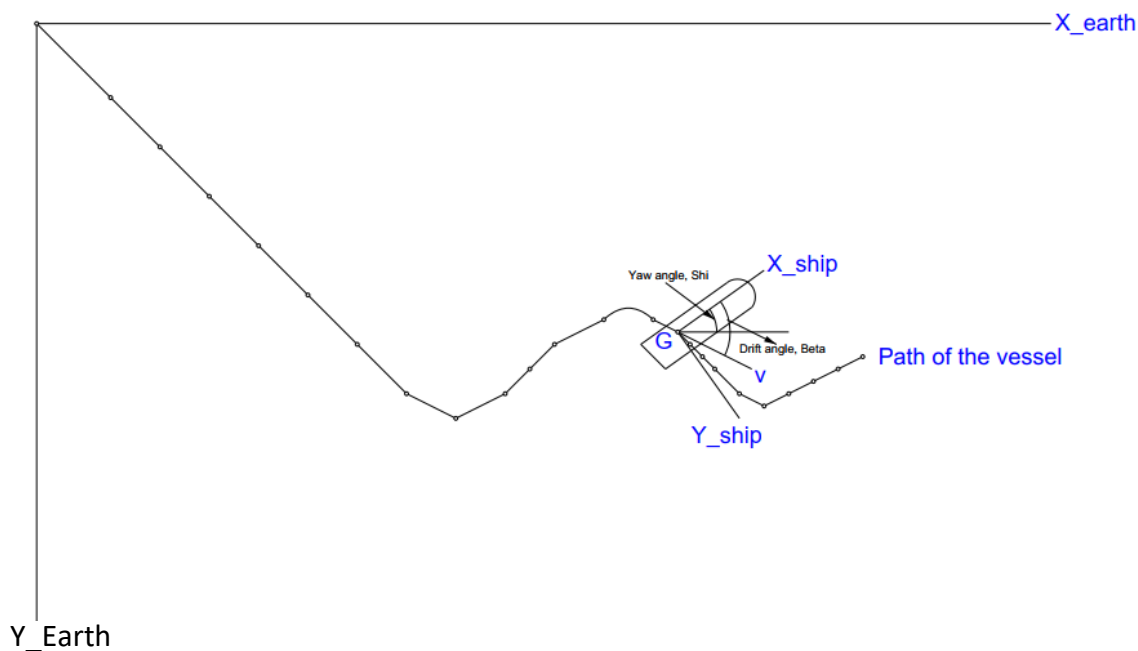


Figure 3: Coordinate system

Let us consider a vessel with the location of center of gravity, G is following the path shown. The X_{earth} and Y_{earth} are the global coordinates in reference to the ship. X_{earth} and Y_{earth} are positive toward right and toward down respectively. The velocity vector of the vessel is v . The X_{ship} and Y_{ship} are the body fixed coordinates in reference to the ship. The yaw angle ψ shows the deviation of the vessel heading which is X_{ship} direction with respect to earth heading which is X_{earth} . The drift angle β is the difference between the vessel heading X_{ship} and the velocity vector v .

For simplicity, let us consider that only sway, surge and yaw moment is acting on the vessel. These three forces are to be identified first is the earth coordinate and a coordinate transformation will be applied to find out these forces in the body fixed coordinate system. The movement in the earth fixed coordinate system is defined by x_{earth} and y_{earth} . The velocity in the earth coordinate system is \dot{x}_{earth} and \dot{y}_{earth} . The acceleration in the earth coordinate system is \ddot{x}_{earth} and \ddot{y}_{earth} . The velocity in the body fixed coordinate system is u and v . The acceleration in the body fixed coordinate system is \dot{u} and \dot{v} . As per Newton's law of motion, the forces on the earth coordinate will be as follows:

$$Surge_{earth} = m\ddot{x}_{earth}$$

$$Sway_{earth} = m\ddot{y}_{earth}$$

$$Yaw_{earth} = I_z\ddot{\psi}$$

Equation 30

In order to transform the forces to the body coordinate system, a basic transformation matrix will be used. From the following figure, is it seen that the angle of deviation is θ .

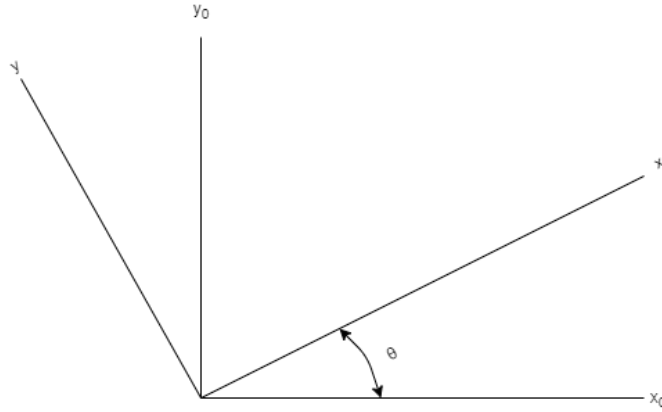


Figure 4: Body Transformation

The transformed and deviated coordinate system can be written as following:

$$x = x_0 \cos\theta + y_0 \sin\theta$$

$$y = y_0 \cos\theta - x_0 \sin\theta$$

Equation 31

In matrix format, it can be written as following:

$$\begin{bmatrix} x \\ y \end{bmatrix} = \begin{bmatrix} \cos\theta & \sin\theta \\ -\sin\theta & \cos\theta \end{bmatrix} \begin{bmatrix} x_0 \\ y_0 \end{bmatrix}$$

$$\begin{bmatrix} x_0 \\ y_0 \end{bmatrix} = \begin{bmatrix} \cos\theta & -\sin\theta \\ \sin\theta & \cos\theta \end{bmatrix} \begin{bmatrix} x \\ y \end{bmatrix}$$

Equation 32

Now, the forces can be transformed from earth to body and it can be written as the following:

$$Surge_{ship} = Surge_{earth} \cos\theta + Sway_{earth} \sin\theta$$

$$Sway_{ship} = Sway_{earth} \cos\theta - Surge_{earth} \sin\theta$$

Equation 33

The intention now is to find out the acceleration in earth coordinate system. It can be written as the following:

$$\begin{aligned} x_{earth}'' &= \frac{d}{dt} [u \cos\psi] - \frac{d}{dt} [v \sin\psi] = \cos\psi \frac{du}{dt} + u \frac{d}{dt} \cos\psi - \sin\psi \frac{dv}{dt} - v \frac{d}{dt} \sin\psi \\ &= \dot{u} \cos\psi + u \frac{d}{d\psi} \cos\psi \frac{d\psi}{dt} - \dot{v} \sin\psi - v \frac{d}{d\psi} \sin\psi \frac{d\psi}{dt} \\ &= \dot{u} \cos\psi - \dot{v} \sin\psi - \psi (u \sin\psi + v \cos\psi) \end{aligned}$$

Similarly,

$$y_{earth}'' = \dot{u} \sin\psi + \dot{v} \cos\psi + \psi (u \cos\psi + v \sin\psi)$$

Equation 34

Replacing the acceleration in the main Newtons equation, the following format of the equations for surge and sway in earth coordinate are achieved.

$$\begin{aligned} Surge_{earth} &= m\dot{u}\cos\psi - m\dot{v}\sin\psi - m[\dot{\psi}(u\sin\psi + v\cos\psi)] \\ Sway_{earth} &= m\dot{u}\sin\psi + m\dot{v}\cos\psi + m[\dot{\psi}(u\cos\psi + v\sin\psi)] \end{aligned}$$

Equation 35

After transforming the coordinate system from earth to body fixed system, the following set of equations are found:

$$\begin{aligned} Surge_{ship}\cos\psi - Sway_{ship}\sin\psi &= (m\dot{u} - m\dot{v}\psi)\cos\psi - (m\dot{v} - m\dot{u}\psi)\sin\psi \\ Surge_{ship}\sin\psi + Sway_{ship}\cos\psi &= (m\dot{u} - m\dot{v}\psi)\sin\psi + (m\dot{v} - m\dot{u}\psi)\cos\psi \end{aligned}$$

Equation 36

Equating the similar terms from the above equation. The following format of the equation is found:

$$\begin{aligned} Surge_{ship} &= (m\dot{u} - m\dot{v}\psi) \\ Sway_{ship} &= (m\dot{v} - m\dot{u}\psi) \end{aligned}$$

Equation 37

After adding the vessels own center of gravity, G the initial set of motion equation in simplified form for Surge, Sway force and Yaw moment of the ship can be written as following:

$$\begin{aligned} Surge_{ship} &= m(\dot{u} - v\dot{\psi} - x_G\ddot{\psi}) \\ Sway_{ship} &= m(\dot{v} - u\dot{\psi} + x_G\ddot{\psi}) \\ Yaw_{ship} &= I_z\ddot{\psi} + m[x_G(\dot{v} + u\dot{\psi})] \end{aligned}$$

Equation 38

2.3.2 Mathematical Model

Yasukawa et al. (Yasukawa, 2015) [\[37\]](#) introduced the MMG standard method for initial prediction of the maneuvering motion. The author shows the hydrodynamic derivatives acting on the hull force and also showed in the non-dimensional form. The set of equations provided by the author are shown below:

$$\begin{aligned}
X_H &= \frac{1}{2} \rho L_{pp} dU^2 X'_H(v'_m, r') \\
Y_H &= \frac{1}{2} \rho L_{pp} dU^2 Y'_H(v'_m, r') \\
N_H &= \frac{1}{2} \rho L_{pp}^2 dU^2 N'_H(v'_m, r')
\end{aligned}$$

Equation 39

Here, v'_m, r' are nondimensionalized lateral velocity and nondimensionalized yaw rate respectively. After expanding the parameters to appropriate Taylor expansion order, the following equation is generated.

$$\begin{aligned}
X'_H(v'_m, r') &= -R'_0 + X'_{vv} v'_m{}^2 + X'_{vr} v'_m r' + X'_{rr} r'^2 + X'_{vvvv} v'_m{}^4 \\
Y'_H(v'_m, r') &= Y'_v v'_m + Y'_R r' + Y'_{vvv} v'_m{}^3 + Y'_{vvr} v'_m{}^2 r' + Y'_{vrr} v'_m r'^2 + Y'_{rrr} r'^3 \\
N'_H(v'_m, r') &= N'_v v'_m + N'_R r' + N'_{vvv} v'_m{}^3 + N'_{vvr} v'_m{}^2 r' + N'_{vrr} v'_m r'^2 + N'_{rrr} r'^3
\end{aligned}$$

Equation 40

The coupled terms above in the equation set are known as hydrodynamic derivatives.

Aslan (Aslan, 2015) [\[38\]](#) developed a MATLAB based numerical simulation technique that can predict maneuvering simulation. The author analyzed the available maneuvering prediction model and then developed his own model based on empirical equations by Lewandowski, Denny & Hubble.

The Lewandowski equation, Denny & Hubble equation equations are given below:

$$\frac{STD}{L} = [1.7 + 0.0222 F_V \left(\frac{L}{\frac{1}{\sqrt{3}}} \right)^{2.85}] \left(\frac{30}{\delta} \right)$$

Equation 41

The equation is valid with in a range of 0.3 – 0.4 of F_V and 4.5 – 7 of $\frac{L}{\frac{1}{\sqrt{3}}}$. F_V is defined by $\frac{U}{\sqrt{g \left(\frac{1}{\sqrt{3}} \right)}}$

The Denny & Hubble equation is given below where U_A and U_C are approach and steady speed respectively:

$$\frac{R_c}{L} = \left[\frac{1}{\left(\frac{U_A}{U_C} \right)^2 - 1} \right]^{\frac{1}{2}} F_V \left(\frac{30}{\delta} \right)$$

Equation 42

Bhawsinka (Bhawsinka, 2011) [39] developed 6 DoF motion equation with coupled parameters. The mathematical model proposed in the research paper is widely used by researchers across the world and used write commercial codes for simulation as well. The surge, sway and heave force are defined by X_{surge} , Y_{sway} and Z_{heave} respectively. The roll, pitch and yaw moment are defined as K , M and N respectively. X_G , Y_G and Z_G are the location of center of gravity in X, Y and Z direction respectively. U, V and W are surge, sway and heave velocities respectively. ϕ , θ and ψ are roll, pitch and yaw angle respectively. M is the mass of the vessel and I_{ij} are the inertia in matrix format. These equations are the finalized equation to simulation the behavior of the vessel during maneuvering condition.

$$X_{surge} = M[\dot{u} + wq - vr - X_G(q^2 + r^2) + Y_G(pq - \dot{r}) + Z_G(pr + \dot{q})]$$

$$Y_{sway} = M[\dot{v} + ur - wp - Y_G(p^2 + r^2) + Z_G(qr - \dot{p}) + X_G(qp + \dot{r})]$$

$$Z_{heave} = M[\dot{w} + vp - uq - Z_G(p^2 + q^2) + X_G(rp - \dot{q}) + Y_G(rq + \dot{p})]$$

$$K = I_{xx}\dot{p} + I_{xy}(\dot{q} - pr) + I_{xz}(\dot{r} + pq) + I_{yz}(q^2 - r^2) + (I_{zz} - I_{yy})qr + m\{Y_G[\dot{w} + vp - uq] - Z_G[\dot{v} + ur - wp]\}$$

$$M = I_{yy}\dot{q} + I_{yz}(\dot{r} - pq) + I_{yx}(\dot{p} + qr) + I_{zx}(r^2 - p^2) + (I_{xx} - I_{zz})rp + m\{Z_G[\dot{u} + wq - vr] - X_G[\dot{w} + vp - uq]\}$$

$$N = I_{zz}\dot{r} + I_{zx}(\dot{p} - rq) + I_{zy}(\dot{q} + rp) + I_{xy}(p^2 - q^2) + (I_{yy} - I_{xx})pq + m\{X_G[\dot{v} + ur - wp] - Y_G[\dot{u} + wq - vr]\}$$

Equation 43

2.4 Crash Stop

After the maneuvering motion, the study focus was shifted to find out the track reach for a crash stop distance. The crash stop starts with an astern order of the engine and propeller. Sometimes a rudder correction is performed but in this study the computation or the simulation will be carried out without rudder correction. The prime concern at this case, was to implement the correct time lag for engine order to execution.

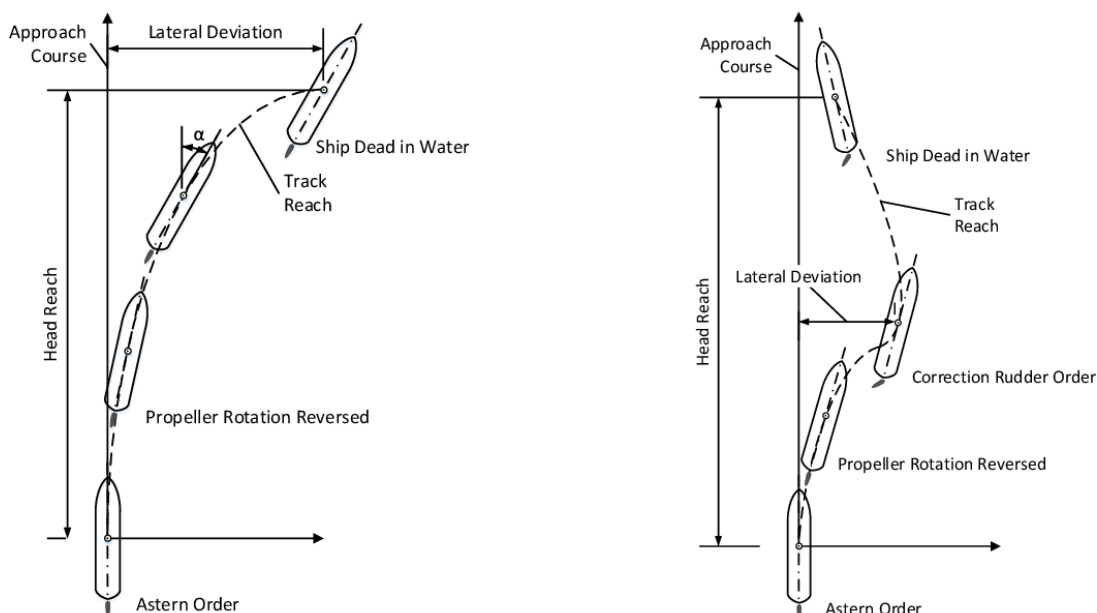


Figure 5: Crash stop of a vessel

[Image Source : <https://www.semanticscholar.org>] ^[40]

Wang et al. (Wang, 2020) ^[41] studied for stopping maneuvering in CFD using the overset grid technique. The author developed their own CFD solver to study the stopping behavior. The author performed the computation with an overset grid with rudder and hull domain. The experiments and the CFD simulations show agreeable results in case of track reach. However, the vessel in this case is a KVLCC which is a heavy displacement vessel.

Varyani et al. (Varyani, 2009) ^[42] studied for stopping maneuvering specifically for high-speed vessels fitted with propeller and waterjet. The author showed an equation of motion for a vessel fitted with propeller by the following equation:

$$\frac{\Delta(1 + k_1)}{g} \frac{dU}{dt} = -T(n, U, t) - R(U)$$

Equation 44

Here, T is the propeller thrust and R is the vessel resistance, k_1 is the longitudinal added mass coefficient. The track reach can be solved using the following equation in general:

$$S_T = \left[\frac{\Delta(1 + k_1)U_0^2}{2gR_0} \log_e \left(1 + \frac{R_0}{T_A} \right) \right] + 0.5U_0t_r$$

Equation 45

In the above equation, U_0 is the ahead speed, T_A is the aft ward thrust R_0 is the ahead resistance.

Park et al. (Park, 2020) [43] studied for stopping maneuvering specifically for ships equipped with azimuth propeller. The author compared the achieved result with a full-scale trial. The data obtained in the paper are valuable in the sense of comparing with the simulated result only for azimuth propeller. Oneto et al. (Oneto, 2017) [44] researched on the basis of full-scale trial data and tried a predication method for crash stopping with artificial intelligence. Yabuki et al. (Yabuki, 2006) [45] researched on stopping motion during a maneuvering for a CPP equipped vessel under windy condition. The author performed simulation and full-scale test in order to validate the results. It was found that the turning motion is less stable in CPP than a FPP.

Sun et al. (Sun, 2018) [46] researched on the possibility of finding the track reach distance for a heavy displacement vessel using numerical simulation. The author developed their own RANS solver model. The vessel taken as reference to compare with is KVLCC2 since this vessel has experimental data available. The author proposed the equation of motion for stopping. This is similar to the maneuvering equation of motion but has some extra terminologies related to total drag coefficient and hydrodynamic derivatives.

$$\begin{aligned} X &= -m_x \dot{u} - \frac{1}{2} \rho S_W C_T u^2 + X_{\beta\beta} \beta^2 + (X_{\beta r} - m_y V) \beta \gamma + X_{rr} r^2 + X_{\beta\beta\beta} \beta^3 + X_p \\ Y &= -m_y \dot{v} + Y_{\beta} \beta + (Y_r - m_x u) r + Y_{\beta\beta} \beta^2 + Y_{\beta r} \beta^2 r + Y_{rrr} r^3 + Y_p \\ N &= -J_{zz} \dot{u} + N_{\beta} \beta + N_r r + N_{\beta\beta} \beta^2 + N_{\beta r} \beta^2 r + N_{rrr} r^3 + N_p \end{aligned}$$

Equation 46

The terms represent their usual meaning with the coupled terms meaning the hydrodynamic derivatives. The author used SST K – ω turbulence model for the simulation. The author finds very good approximation for the experimental data and the simulated data.

Ming et al. (Ming, 2013) [47] studied on finding the empirical formulation for vessel stopping distance and the vessel crash stopping distance. Since the current research is not dealing with any sort of aft ward thrust, the focus will remain on the stopping distance. The terminologies adopted in the equation are as follows: k is the vessel virtual mass coefficient, V_t is the final speed, V_0 is the initial speed and M is the vessel mass. The equation for time to stop and the stopping distance is given below:

$$\begin{aligned} t_s &= \frac{M}{k} \left(\frac{1}{V_t} - \frac{1}{V_0} \right) \\ S_s &= \frac{M}{k} (\ln V_0 - \ln V_t) \end{aligned}$$

Equation 47

Duman et al. (Duman, 2021) [48] predicted the stopping maneuver for a DTMB high speed bare hull using closed form analytical solution and CFD. The author found good approximation with the experimental data.

Tani (Tani, 1968) [49] studied the stopping maneuver and the time lag between the signal execution. The author neglected the slip of propeller in this case.

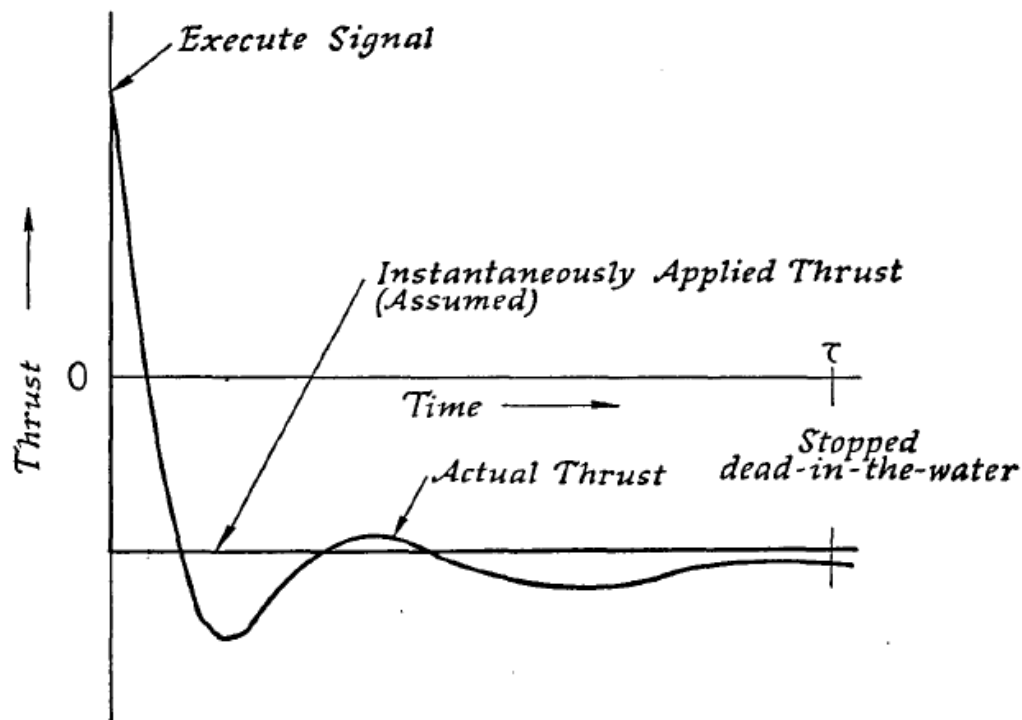


Figure 6: Time execution for stop order

[Image Source : Tani (Tani, 1968) [49]]

The equation of motion in this case is written as following:

$$(m + m_x) \frac{du}{dt} + (m + m_y) \omega \nabla = -R - T$$

Equation 48

The second term on the left-hand side denotes the component for centrifugal force and it can be considered inside total resistance or the aft ward thrust.

Norrby (Norrby, 1968) [50] studied the retardation factor during the stopping maneuver of merchant vessel. However, the technique seems promising and can be applied to high-speed vessel with some caution. For example, the author conducted the test for a single screw ship and in order to apply it to twin propeller vessel, an interaction factor is required. The author proposed an integral formulation from which the time taken to stop can be determined. The k_x in the equation is known as added mass coefficient.

$$\frac{\nabla}{g}(1 + k_x) \frac{dV}{dt} = -F$$

Equation 49

Gan et al. (Gan, 2013) [51] studied the Topley formulation and proposed a new empirical method for crash stopping distance. The method can be applied to heavy displacement vessels but can be applied to medium speed vessel with caution. If the stopping distance is S_j , the equation can be seen as follows.

$$S_j = \frac{\left[\left(v_1 \cdot -C \log_2 \left(\frac{v_1}{v_0} \right) + \frac{C(v_0 - v_1)}{0.693} \right) \left(1 - 2^{\log_2 \left(\frac{v_1}{v_0} \right)} \right) \right]}{60}$$

Equation 50

Here, v_0 is the initial speed and v_1 is the speed at the time of stopping the engine. C is known as the time halved constant of ship's speed and can be calculated according to the following table provided by the author.

Table 1: Time halved constant of ship's speed

Tonnage	C (min)	Tonnage	C (min)	Tonnage	C (min)
1000	1	36000	8	120000	15
3000	3	45000	9	136000	16
6000	3	55000	10	152000	17
10000	4	66000	11	171000	18
15000	5	78000	12	190000	19
21000	6	91000	13	210000	20
28000	7	10500	14		

Figure 7: Table for finding the value of C

[Image Source : Gan (Gan, 2013) [51]]

Okamoto et al. (Okamoto, 1974) [52] studied the stopping ability for a vessel with CPP arrangement and checked the result with an experimental setup. The results were further compared with the FPP arrangement. From the experimental setup the authors concluded that the CPP arrangement has better stop ability compared to FPP as aft thrust can be generated with less time by changing the blade angles.

Ueno et al. (Ueno, 2017) [53] conducted numerical simulation and towing tank test. The author used the simplest one degree of freedom motion equation and also tried to find the propeller forces due to reversing the propeller. The author proposed an advance speed, J and speed correction for the vessel as well.

Harvald (Harvald, 1976) [54] conducted tests and concluded that the optimum propeller for the propulsion will also be the most suitable one for stopping the vessel. The vessel also concluded that the coasting or windmilling with the propeller with the largest possible diameter and least possible pitch will be the most suitable for stopping.

2.5 Turbulence Model

Liu et al. (Liu, 2015) [\[55\]](#) introduced hybrid mesh technique with overset in order predict the maneuvering motion of the vessel. The author conducted a planer motion mechanism (PMM) to find out the hydrodynamic derivatives. The results showed good agreement with experimental data.

Karim et al. (Karim, 2011) [\[56\]](#) showed $k - \omega$ SST model is better to capture and predict the flow near as well as far from the boundary. The simplified boundary layer equation fails to predict flow in the stern and in the wake field and it is believed because of inaccurate turbulence model. The author used SST $k - \omega$ model to simulate the flow around the object. The SST model uses $k - \omega$ model near the solid wall and uses $k - \varepsilon$ model away from the wall by using a blending function. The model also considers the turbulent shear stress transport. Viscosity is modified in order to account for principle sheer stress. This allows the model to be used in the boundary layer to the body through all the viscous sublayers. The model includes a cross diffusion term and blending function giving it the advantage over standard $k - \omega$ and $k - \varepsilon$ model. Hence it can be implemented correctly in the Boundary and the far field domain and computation can be reduced by not solving the $k - \omega$ equation in the far field boundary.

Chapter 3 Methodology, Simulation and Validation

In this chapter, the methodology for the calculation will be mentioned in detail. As mentioned earlier, a commercial software named, FineMarine will be used to simulate the turning circle maneuvering. The commercial software has its own meshing tool named HExpress and the RANS solver is based on ISIS-CFD. The ISIS-CFD code is developed by LHEEA of Ecole Centrale de Nantes. An octave program has been developed in order to find the turning circle and also to find other parameters as required. The program is attached as an [appendix](#) on the end of the report.

3.1 CFD and Overset Mesh

With increasing computation power at a reasonable price, using of CFD solver for solving complex mathematical problem skyrocketed. Many research and professional works are being carried out in CFD solver now a days. With more validation tools available and the methodology being verified with experiments, many approaches were taken on computation with CFD solver.

Finding the resistance or drag force of a ship is nothing exceptional in this case. The ship is faced with viscous frictional resistance and wave resistance. Wave resistance has two more components and they are wave breaking and wave field resistance. The maneuvering problem is same as classical resistance but in this case the CFD is used to compute the forces and motions of the vessel.

The classical meshing approach is unsuitable to solve this type of computation. It is possible to have broken computation since mesh deformation is quite high as the vessel will make maneuver. For this reason, overset mesh is preferred for this type of calculation. An overset domain allows mesh deformation and allows cell to cell data exchange.

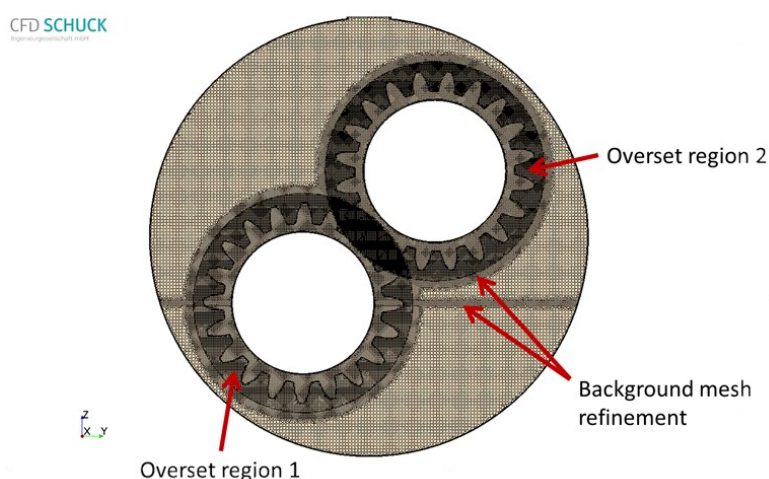


Figure 8: Typical Overset Domain

[Image Source: <https://www.hpctoday.com>]

3.2 Mesh and RANSE Solver

The mesh modelling performed in the thesis was with the help of a commercial mesh generation software named HExpress. Based on the website data, the software generates non-conformal body-fitted full hexahedral unstructured meshes on complex arbitrary geometries. Apart from that, the advanced smoothing capability provides high-quality boundary layers insertion. It was also found that the HEXPRESS™ uses a volume-to-surface approach, suppressing the need for a surface mesh.

Regarding the flowsolver, The ISIS-CFD flow solver, uses the incompressible unsteady Reynolds-averaged Navier Stokes equations (RANSE). The solver uses finite volume method to build the spatial discretization for transport equations. The velocity field is obtained from the momentum conservation equations and the pressure field can be extracted from the mass conservation constraint, or continuity equation, transformed into a pressure-equation.

3.3 Meshing Methodology

The meshing methodology starts with the preparation for the domain. As there will be overlapping domains, it was necessary to model each domain block separately.

3.3.1 Domains

In total four domains are required to be created. They are listed as follows:

- Two Rudder Domains
- One Hull Domain
- One Background Domain

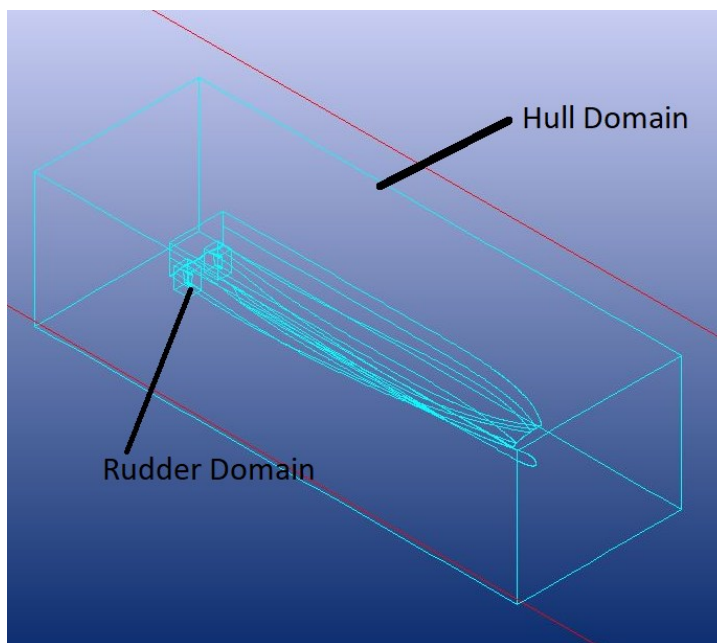


Figure 9 Hull and Rudder Domains

The reason for three separate domains is because we are dealing with high mesh deformation. This is not possible to capture with regular setting. As a result, three separate domains with overlap configuration are required.

- Two phases are required to simulate the Turning Circle. The first one is acceleration and the second one is the turning phase where the vessel and the rudder will rotate.
- There will be large deformation of mesh during turning of rudder as well as the vessel.
- Since this is not possible to do correctly with default weighted deformation by Fine Marine, overlapping domain is required.

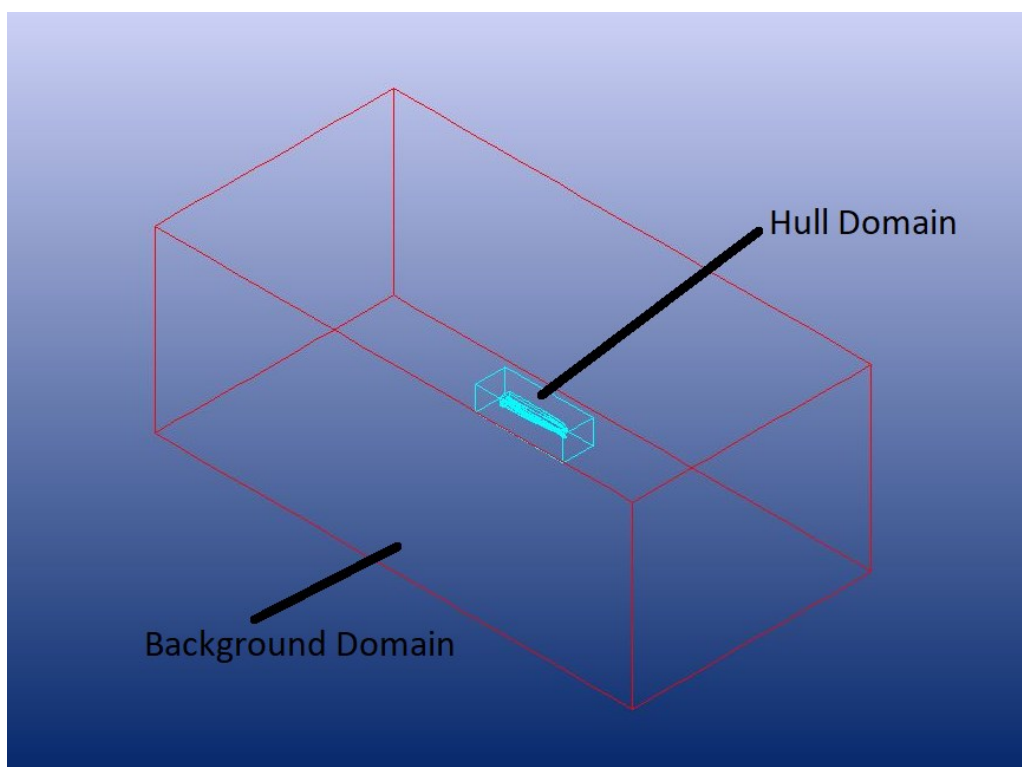


Figure 10 Hull and Background Domain

In order to make sure proper cell to cell data transition, an ideal cell size ratio was ensured. To do so, all four domain's size was calculated. The target was to ensure round number of cells inside each domain. For this reason, an initial cell size for background was calculated.

From the background cell size, further refinement led to find the hull and rudder domain initial cell size. By putting round numbers of cells in all four domains, the final domain size was found.

Table 5: Domain size (brief)

Domain size (in multiplication of L_{pp} [except Rudder])			
Parameter	Background	Hull	Rudder
Length	8	1.5	1.5 x length of long edge
Breadth	4	3	9 x maximum thickness
Height	3	3	2 x rudder height

The following table shows the domain size that was used throughout the computation for this specific case.

Table 6 Value of Domain Size (Rudder)

Domain Name	Parameter	Value
Rudder	Xmin	-0.25 x Long Edge Length
	Ymin	-4.5 x Maximum Thickness
	Zmin	-0.5 x Height
	Xmax	1.25 x Long Edge Length
	Ymax	4.5 x Maximum Thickness
	Zmax	1.5 x Height
Domain Name	Parameter	Value
Hull	Xmin	-0.25 x Lpp
	Ymin	-1.5 x Breadth
	Zmin	-1 x Depth
	Xmax	1.25 x Lpp
	Ymax	1.5 x Breadth
Domain Name	Parameter	Value
BG	Xmin	-4 x Lpp
	Ymin	-2 x Lpp
	Zmin	-1.5 x Lpp
	Xmax	4 x Lpp
	Ymax	2 x Lpp
	Zmax	1.5 x Lpp

The following pictures shows a reference length depiction based on the table provided earlier.

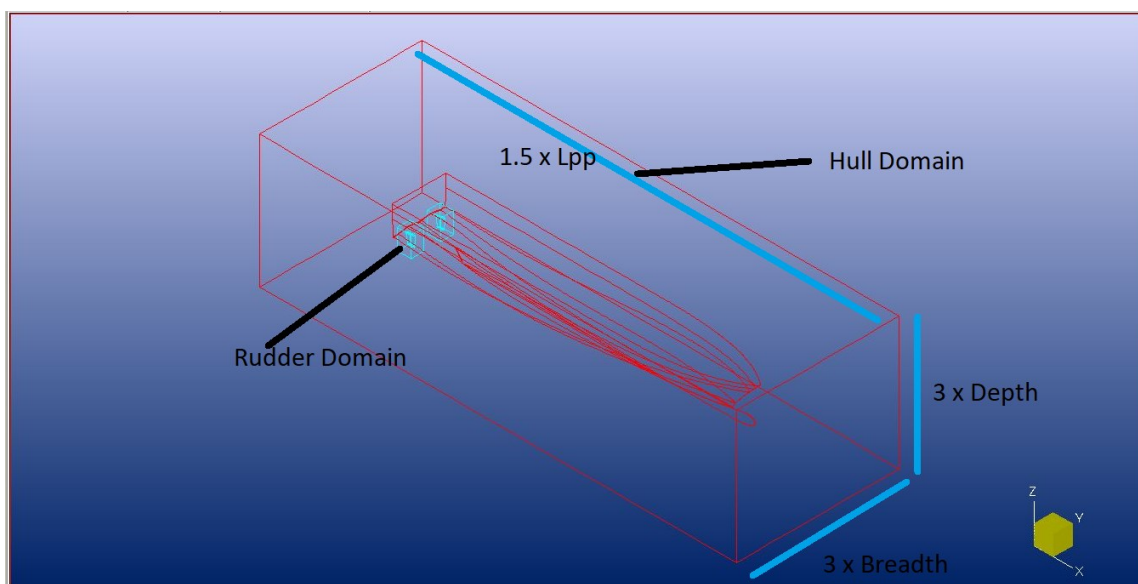


Figure 11: Domain Size [shown for hull as reference]

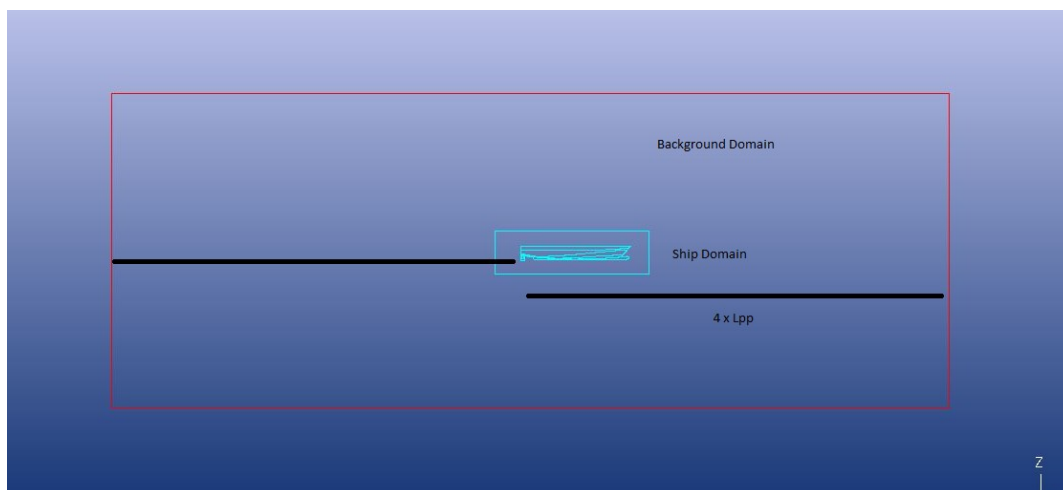


Figure 12: Domain Locations [Profile View]

The reason to find out a perfect domain size is associated with the cell size ratio. As per Numeca, when a cell is flagged for refinement, it is advisable to also tag its neighbours for refinement in order to ensure a sufficiently smooth transition between fine and coarse cell regions. This process is called "refinement diffusion". The diffusion at the boundary should be uniform as shown in the following picture:

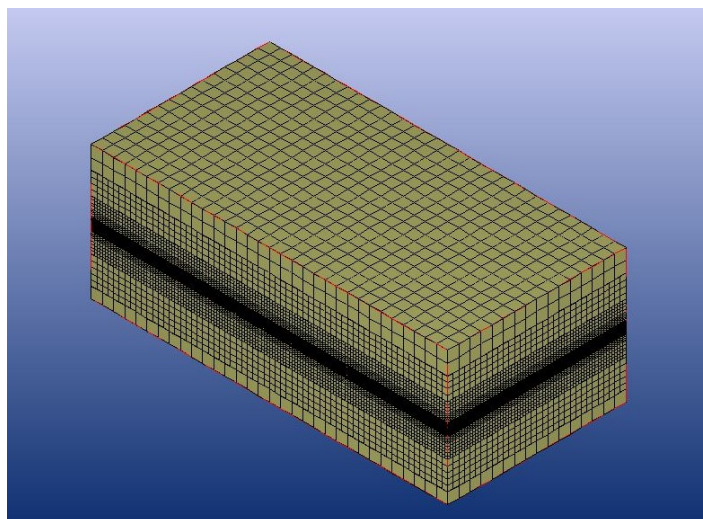


Figure 13: Uniform cell diffusion

The prime intention from a simulation designer's point of view was to reduce cost for meshing and reduce the computation time. This means an overall reduction of computation cost on a global scale. In this section, the target was to reduce the mesh size as much as possible. The software used in this case has two generalized steps for generating the mesh. These are initial cell size and mesh adaptation.

After completing the meshing procedure, the domain is checked for orthogonality and expansion ratio. FineMarine suggests to keep the maximum expansion ratio below 20 and orthogonality above 10 degrees.

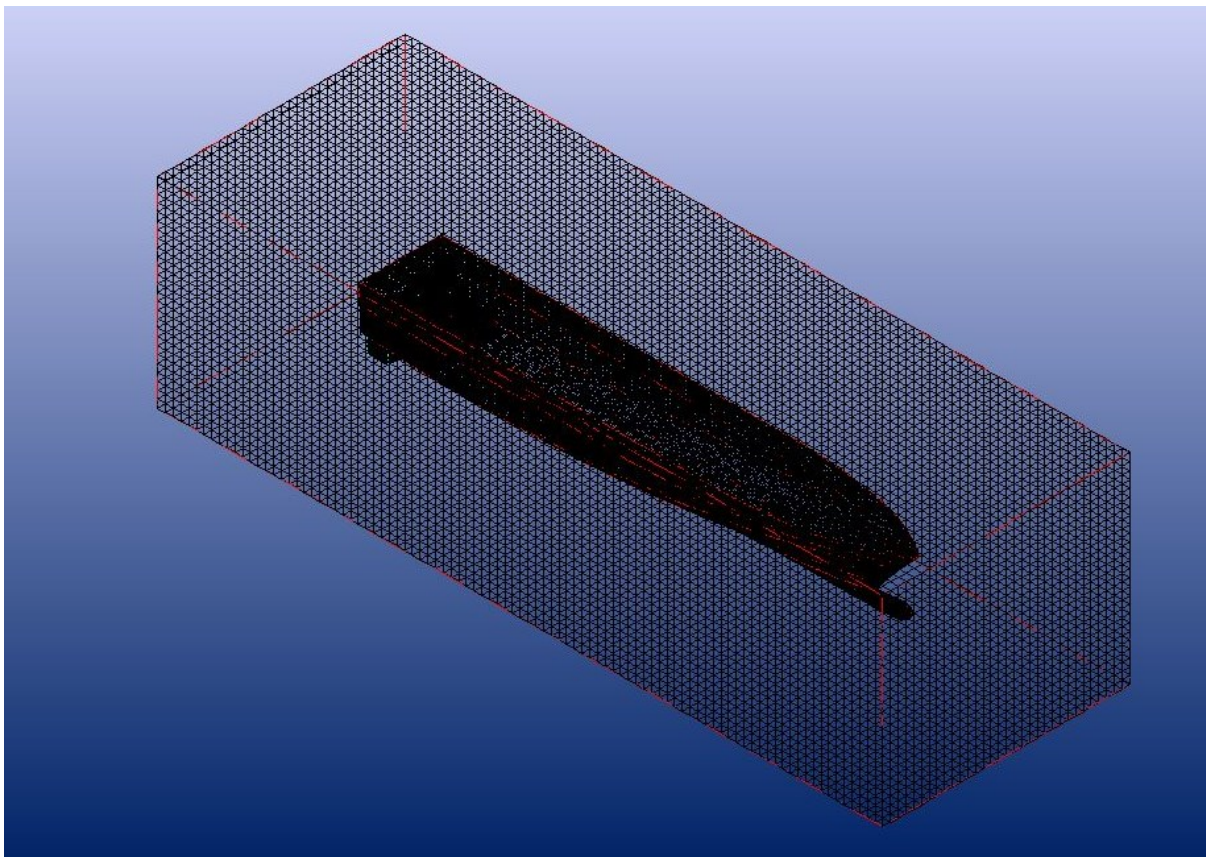


Figure 14: Hull Domain [After Meshing]

The following figure shows a cut plane after meshing. The high refinement zone near the bow curve and the stern is visible. The refinement is required to allow the CFD solver to accurately solve the flow near this region.

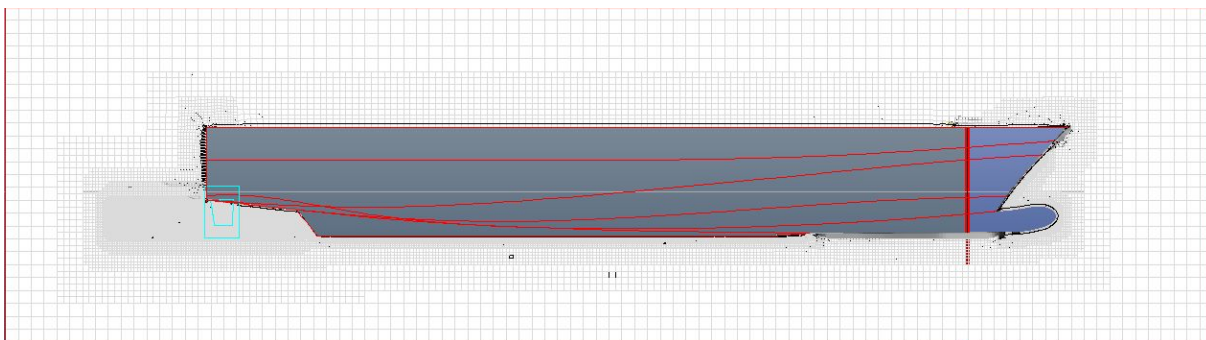


Figure 15: Hull Domain Cut Plane [After Meshing]

3.3.2 Initial Cell Size

The meshing technique starts with the procedure by applying an initial cell size over the domain. The background domain is by default the reference for all domain. The initial cell size obtained here is refined in order to have other domain's cell size. The formulation depends on different factors but in the case of this specific software, the following formulation was used to find out the cell size for background, ICS_B :

$$ICS_B = \frac{1000}{L_{pp}} * 2^8$$

Equation 51

The initial cell size for hull and rudder domain are given in the following sets of equations. The hull and rudder domains are refined 4 and 8 times respectively.

$$ICS_H = \frac{ICS_B}{2^4}$$

Equation 52

$$ICS_R = \frac{ICS_B}{2^8}$$

Equation 53

From the above formulations and use of the above table, the initial cell number can be found with some simple calculation. The best practice is to have a round number of cells in all X, Y and Z direction in order to have uniformity. Having a round number cell will slightly increase the domain size from the previous assumption.

The cell number (N) and the new coordinate (X/Y/Z) can be easily found with the following formulations:

$$N_B = \frac{X_{Max} + X_{Min}}{ICS_B}$$

Equation 54

The new coordinate will be as following:

$$X_{min(new)} = X_{min(old)}$$

$$X_{max(new)} = X_{min(new)} + (\text{cell size} * \text{rounded cell number})$$

Equation 55

3.3.3 Mesh Adaptation Technique

This section deals with the procedure to adapt the mesh at each poly-surface from the initial cell size. This is where the designer needs to apply the refinement level and choose appropriate value for refinement. Wrong value or wrong evaluation of the surface may lead to excessive number of cells increasing the time and mesh cost. In a vessel, there will be different areas or surfaces where a number of refinements needs to be applied. General idea is to apply higher refinements where high flow interaction and high flow separation may be identified. An example could be the rudder leading edge or keel thickness etc.

For this specific problem, the location of the propeller disk has to be refined by creating a section. This area will contain the ‘Actuator disk’ in the flow solver. The target for refinement is to ensure uniform mesh to have correct force distribution.

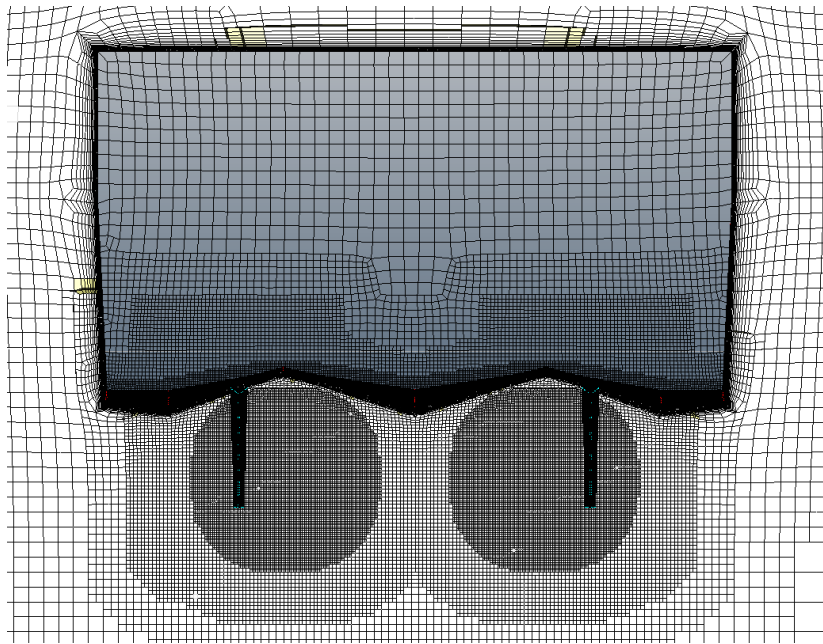


Figure 16: Refinement Sector near propulsion device

Another set of refinement sector is required to direct the flow towards the propeller and rudder. As seen from the following picture, a reference flow refinement sector is shown for the port side.

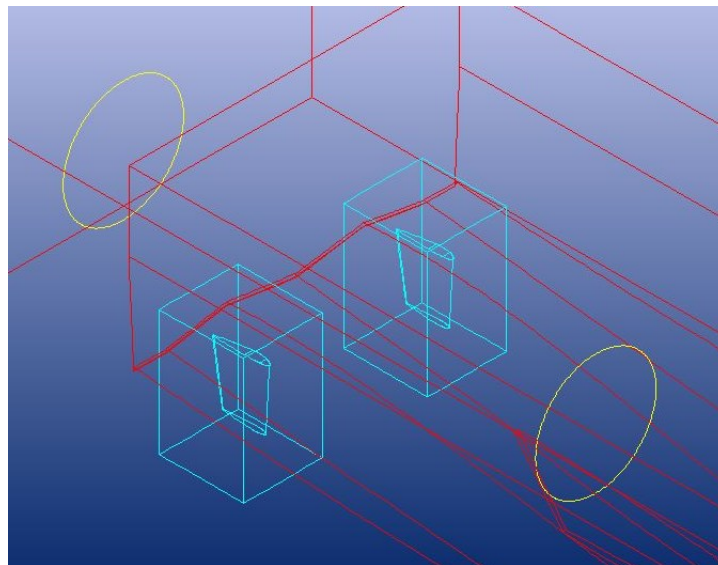


Figure 17 Flow refinement sector

A refinement box with same size of hull domain and two refinement boxes with same size of rudder domains are created in order to ensure perfect cell to cell ratio. This will help to transfer cell to cell information much more efficiently.

3.3.4 Viscous Layer Addition

The remaining task at this section is to add the viscous layer on the surfaces based on the y^+ value where the RANS equation will be solved. A Y^+ value has to be selected carefully or an automated calculation by the software itself can be taken as reference for the computation. The idea is to skip the buffer layer.

$$Y^+ = \max \left\{ y_{Min}^+; \min \left\{ 30 + \frac{(Re - 10^6) * 270}{10^9}; y_{Max}^+ \right\} \right\}$$

Equation 56

The following picture shows the region of each layer in a turbulence model. The viscous sublayer and the log law region has to be followed.

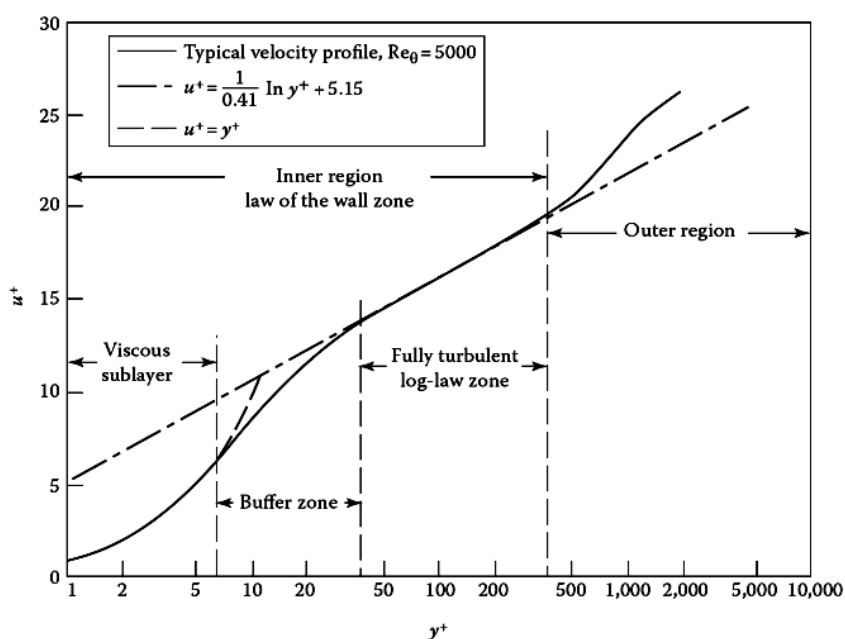


Figure 18: Typical Y^+ regions

[Image Source: Darvish (Darvish, 2015) [\[57\]](#)]

For this particular case, the viscous layer addition was taken as instructed by the FineMarine. It has to be kept in mind that the in-flow velocity for the hull and the rudder is not same. As a result, the Y^+ value will not be same. This will eventually affect the number of viscous layers being added on the solid body. The rudder will have different velocity than the hull due to propeller slip and interaction between the propulsors. There is also a hard chine present on the stern which will also cause a disturbance to the rudder flow.

The following picture shows the formation after the viscous layer being added to the domains.

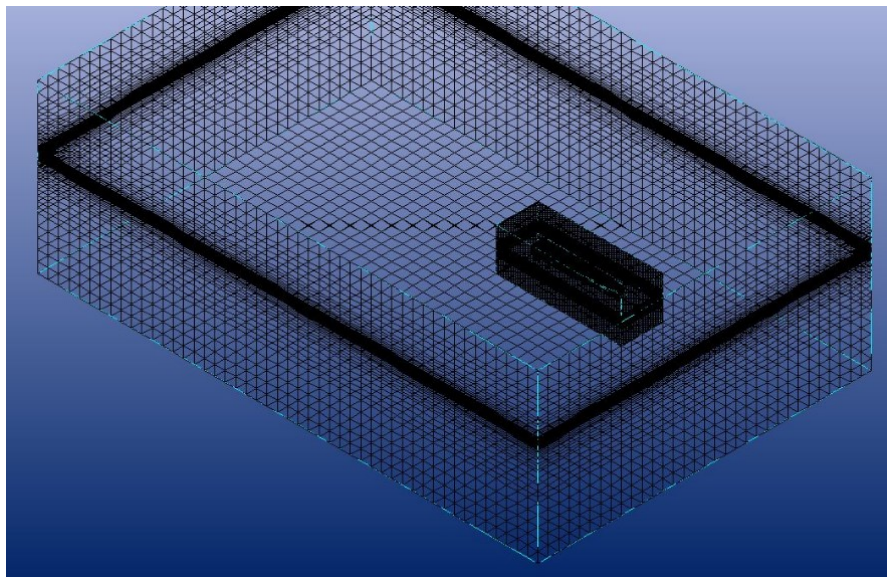


Figure 19 Hull Domain reference with VL

3.4 Simulation Phase

In simulation there will be two phases:

- Acceleration Phase
- Turning Circle Phase

The simulation phase in this case, starts with the acceleration phase. The flow solver code requires a stable equilibrium before moving to the turning circle phase. Numerous efforts were taken in order to reduce the computation time and to reduce the time for each iteration in computation step. These will be discussed in details on the result and validation section.

3.4.1 Acceleration Phase

This section deals with acceleration phase which is the prime requirement for finding out the turning circle and the crash stop. In the acceleration phase, in order to have a proper transition of data between overset boundaries, a cell size ratio of 1 was ensured. The dynamic parameters were given including the inertia matrix.

The hull was given a surge motion with a $\frac{1}{2}$ sinusoidal law acceleration ramp. It took 12 seconds to reach final velocity. Heave and pitch motions were solved in this case and this computation results will be used in the following phase. Some exact parameters were specified including temperature of 19-degree seawater, K omega SST Menter turbulence model. The hull's deck was considered as slip in the boundary condition as solving the viscous flow over there is not necessary. The actuator disk parameters were also given and open water propeller data was given for thrust and torque calculation. Both rudder domains were kept fixed on their position with a rigid connection indicating rudder mid position.

Another important step followed in this step was to work with the adaptive grid refinement (AGR). AGR captures the deformation of the free surface. A refinement zone slightly larger than the hull domain was created in order to ensure the capture.

A uniform time law was selected for the calculation and with trial and error. The acceleration phase is required to be run steady state equilibrium is obtained. In steady state, the drag force, heave and pitch will be converged.

The thrust and torque obtained from actuator disk has to be converged as well. In this case, they were computed using an open water data file. The total simulation time in this particular case was taken as 4 times of the ramp meaning 48 seconds.

3.4.2 Turning Circle Phase

For simulating the turning circle phase, the same acceleration computation results were used but, in this case, all 6 degrees of freedoms were solved for the vessel. Details are mentioned in the result where a comparison is drawn for solving three and six degrees of freedom. The rudder is positioned to 35 degree or a hard over. As a result, the rudder is connected as a pin joint to a reference point in the domain. The time to complete the rudder turning was selected carefully after evaluating the scenario. Rudder execution time depends on rudder shape, size and the hydraulic pumps that are used to perform the task. The thrust and torque data obtained in the acceleration stage will be used in this case.

3.4.2.1 Iteration Stage

At this stage, different trial settings were conducted by varying different parameters. This was the most time consuming and laborious part throughout the process as it requires meshing and then checking for different criteria to be fulfilled.

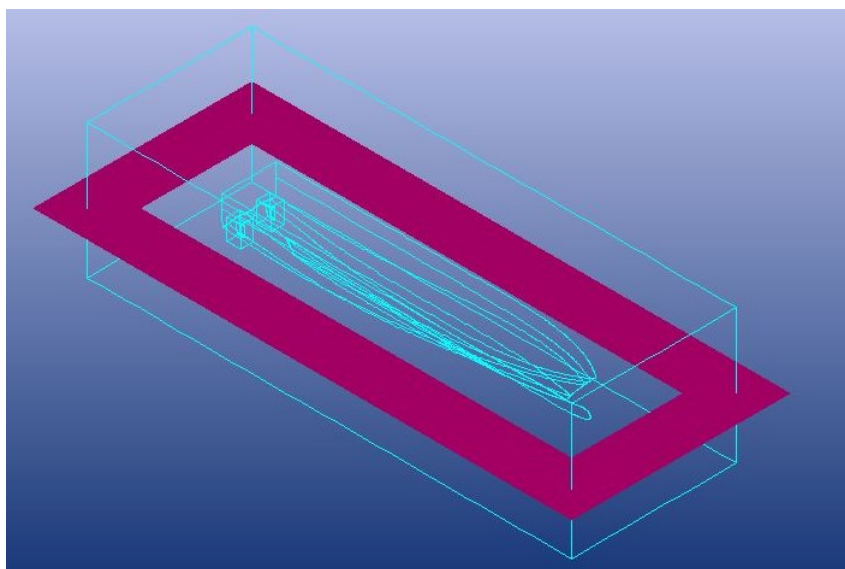


Figure 20 Overlapping boundary refinement at free surface

A tool named “Overset internal surface” from FineMarine was required to ensure proper transition of cell-to-cell data within the deformable zones. The above picture shows the refinement conducted at free surface.

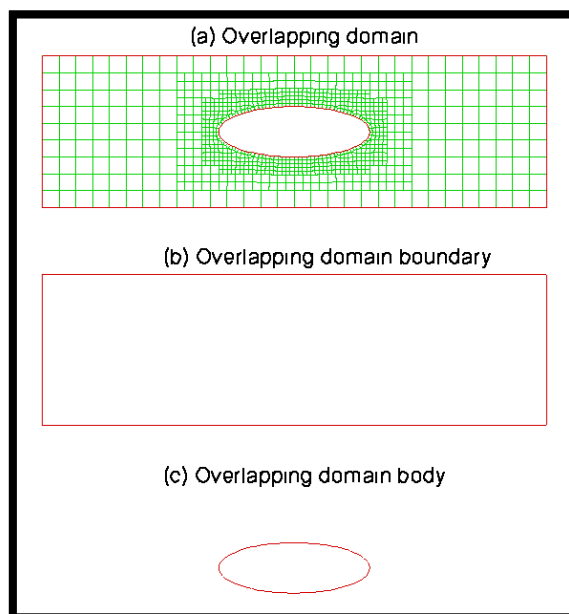


Figure 21 Overlapping Domain

[Image Source: Numeca]

Trial Setting 1:

As a simulation designer, most of the time during the internship was spent to find an optimized balance between performance and accuracy level and off course cost. Initially, a complete mesh size of 12.7 million was generated. The three Overlapping surfaces are placed inside the background domain. The actuator disk location and refinement were also checked. The mesh does not have an exact cell to cell ratio but some computations were performed. The computation on that case failed due to negative volume cell. After that a lot of time was spent to manipulate different parameters and run the computation. In most cases, the computation either failed or taking a lot of time for the time step. The most common two reasons for failing are negative cell volume and grid matching error. In the case of negative cell volume, the mesh was regenerated and a certain number of refinements were applied to probable distorting surface. The grid matching error was being tried to solve by modifying the AGR parameters.

Trial Setting 2:

At this point, the mesh was causing more issues of negative volume. Necessary modifications and parameter changing were conducted for overlapping domains. The actuator disk refinement was kept same. The mesh number at this time was about 12.5 million. In this case also negative volume issues were present. The idea at this stage was to manipulate with the pressure solver since it was believed that the linear pressure solver may be causing the problem. As a result, different combination of pressure solver with orders and iterations were conducted.

Trial Setting 3:

At this point, the main target was to solve the grid matching. As a result, the aspect ratio at overlapping domain boundary were modified and manipulates between suggested number to have a good correlation between the cells. This however was able to solve the grid matching error for a time but negative volume was still causing failing of simulation. The negative volume was believed to be caused by the cell interaction between actuator disk and the rudder domain. The sector size for actuator disk was reevaluated.

Trial Setting 4:

At this point, the actuator disk was still believed to be causing the negative cell volume issue. So, a higher refinement for the actuator disk was applied along with some additional refinements and it increased the cell number to a value of about 14.7 million. This however resolved the issue of negative volume but it took a lot of time for each time step. To be specific, each time step was taking about 7-8 minutes on average and the simulation crashed after a while.

Trial Setting 5:

In order to reduce the computation time, higher NL iterations were given with low orders. Since it was still unable to solve the timing problem, the focus then shifted to adjust the time step size with courant number. A maximum courant number of 0.5 is recommended on the free surface and with the changed time law these parameters were provided. This one is still unable to resolve the high computation time. In order to reduce it a quasi-static approach was also performed.

Trial Setting 6:

With every possible combination, the time problem was not being able to reduce and it was decided to apply certain refinement again at the overlapping boundary (location of free surface between the background and the hull domain).

The free surface target cell size in Z direction was to be refined slightly less as the final refinement to the final target cell size will be refined by AGR. In this case about 11 million cells were generated. However, this was also posing some computation issue.

Trial Setting 7:

In this case, it was noticed the cell-to-cell ratio may not be 1 or close to 1. As a result, the domain size was reevaluated. The computation did run in this case but it was showing some interpolation error initially. It was predicted a slow computation due to not having an exact cell to cell ratio. However, it was not possible to determine its effect since the computation ran perfectly for 3 DOF. The domain size increased and as a result, the number of cells as well. It was 12 million cells in this case.

Trial Setting 8:

The grid criteria settings were reevaluated. The sector disk for actuator were reevaluated. It was decided not to use too fine refinement and adding another sector. The default nonlinear iteration number was taken. A refinement diffusion on the internal free surface was also reduced by level 2. All these combinations drastically reduce the mesh size and bring it to about 8.5 million.

Final Setting:

Refinement boxes were created to ensure proper cell to cell data transition. Mesh uniformity was ensured at the overlapping domain boundaries. The previous setting was still showing few discrepancies and abnormality. As a result, the grid criteria settings were reevaluated with the help and support from FineMarine. Two refinement sectors were proposed in meshing. One is for the location of the propeller disk and another is for the flow refinement. This combination brings the mesh size to about 8.1 million.

Table 7: Comparison between mesh

Changes on each case			
Mesh Serial	Number	Main Feature	Issues
TL 1	about 13.7 million	Overlapping Domains	Negative Volume and Grid matching error
TL 2	about 13.5 million	Overlapping Domains Refinement Box	Negative Volume, Grid matching error, Pressure solver error
TL 3	about 13.5 million	Aspect Ratio	Negative Volume
TL 4	about 14.7 million	Higher refinement to Actuator	NaN Residual
TL 5	about 14.7 million	Time Law and Iteration number	Very high computation time
TL 6	about 11 million	Time Law	High computation time
TL 7	about 12 million	Cell ratio \neq 1	Medium computation time
TL 8	about 8.5 million	Cell ratio = 1 Refinements for actuator disk	Low Computation time but abnormality issue
FS	about 8.1 million	Cell ratio = 1 Two refinement sectors Free Surface target cell size	No Issue Faced for Acceleration and Turning Circle

3.4.3 Crash and Inertia Stop Phase

In contrast to stopping distance calculation, the attention was shifted to finding the inertia stop distance rather than crash stop distance. A propeller blade designed with specific rake and skew angle will not have the same dynamics when rotating on the reverse direction. The complete

dynamics will change as the leading edge will become trailing edge. The angles will also change. As a result, it is sure that the same amount of thrust will not be generated when rotating the propeller in reverse direction.

Due to the computation complexity, physical propeller was not used on the simulation. The reason is complexity and time. The computations performed during this period was conducted on a 128 core CPU. In reference to that, a democase by numeca took 21 days to solve for all 6 dofs and it was also in scale model. The actual thrust imparted during reverse rotation is possible to calculate using CFD by it requires high meshing cost and computation time.

For simulating the inertia stop phase, the same acceleration computation results were used but, in this case also, all 6 degrees of freedoms were solved for the vessel. The rudder is positioned to mid position with the same rigid joint as before. The main challenge in this case was to find out the engine slow down and stop time. A marine diesel engine running at MCR needs careful timing to slow down and stop or eventually apply reverse gear. The thrust and torque data obtained in the acceleration stage will not be used instead a surge motion will be given that eventually makes the speed to zero.

3.5 Result and Validation

After conducting the simulation, the results were obtained. Different plots were seen from the software itself showing various important parameters. Probes were set earlier that will follow the vessel in order to make an animation. Post processing of the results were done by another in built tool names CFView.

3.5.1 Acceleration Phase Result and Graphics

For acceleration phase, the overall drag force in X direction, hereby titled as ‘Fx’ was obtained from the software. A 10% average data for the last few iterations were taken in order to ensure a good convergence. The surge motion, velocity, heave, pitch curves as well as actuator disk data were also obtained. The free surface deviation and hydrodynamic pressure are also seen from the software.

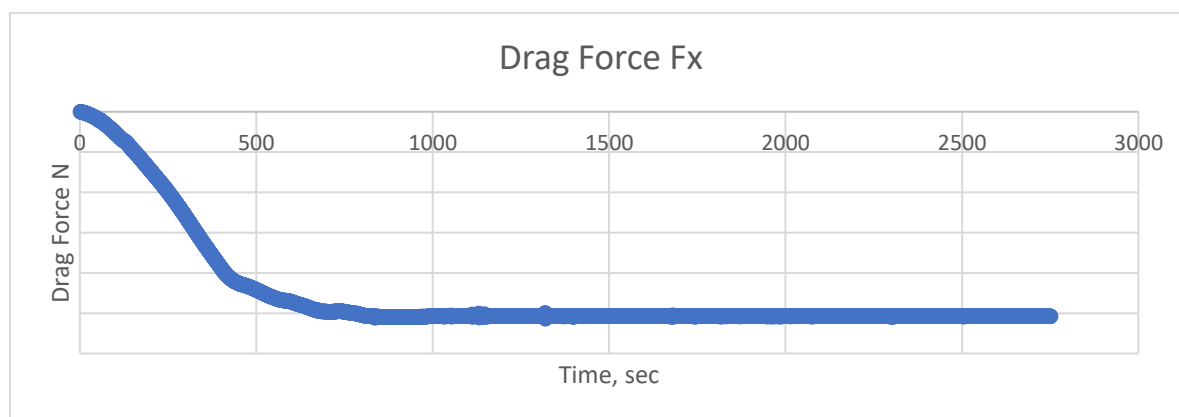


Figure 22: X Direction Drag Force [Acc]

From the above picture it can be seen that the hull force converged to a specific value. The total time step taken in this case was 2751. The system was automated and it could be stopped manually after 40 seconds simulation time.

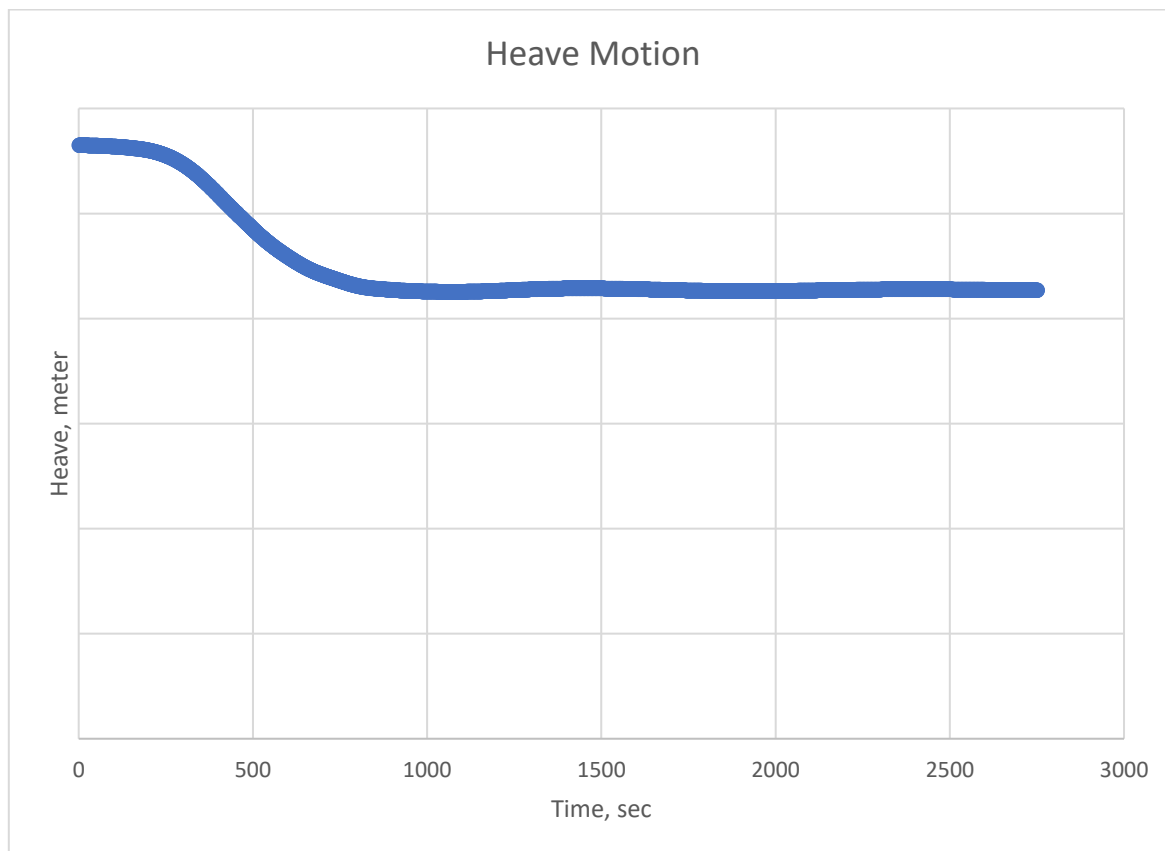


Figure 23: Heave [Acc]

From the above picture it can be seen that the heave motion is also converged to a specific value. The system was automated and it could be stopped manually after 45 seconds simulation time.

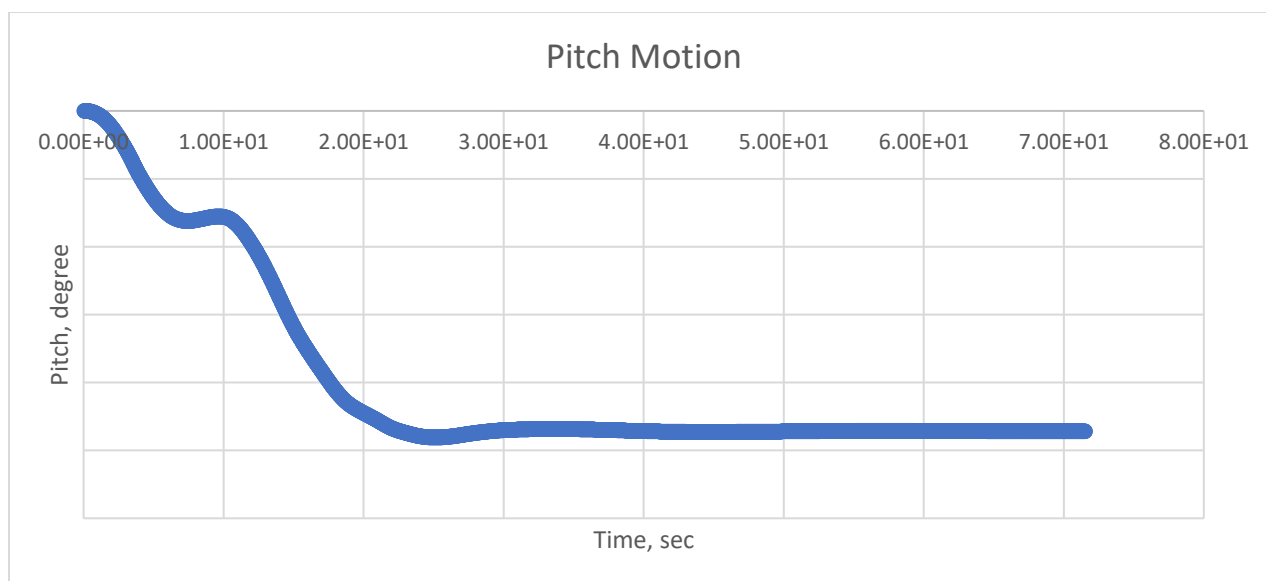


Figure 24: Pitch [Acc]

From the above picture it can be seen that the pitch motion is also converged to a specific value. The system was automated and it could be stopped manually after 45 seconds simulation time.

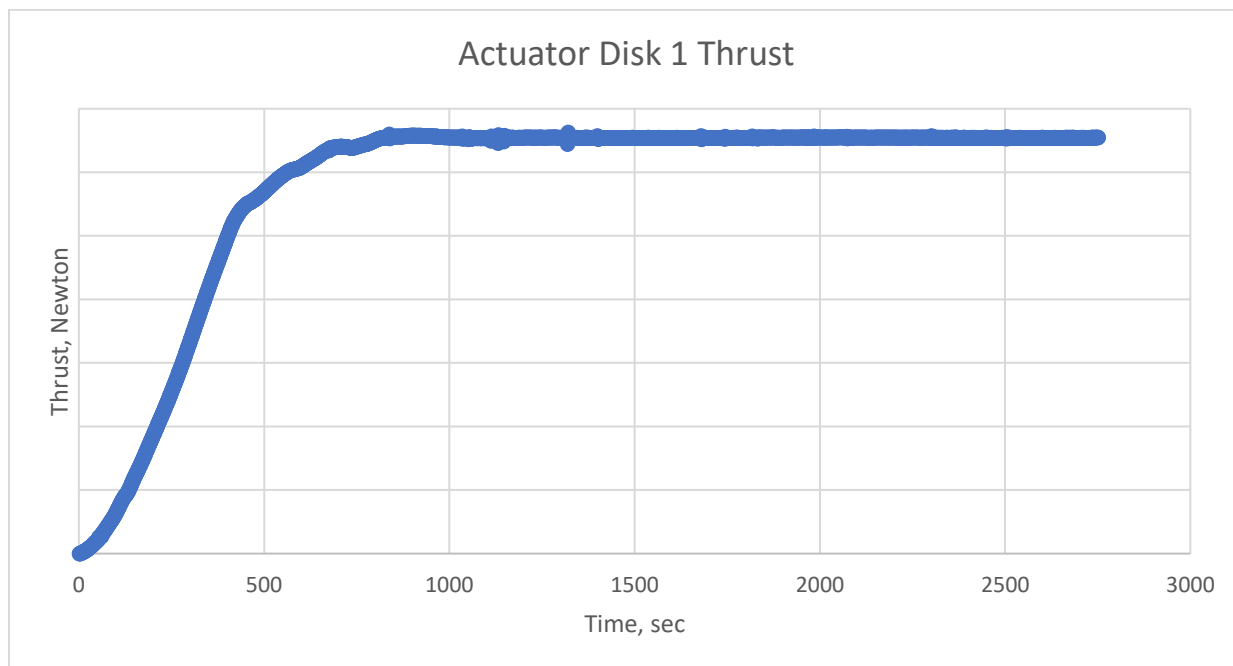


Figure 25: Actuator disk No 1 [Thrust]

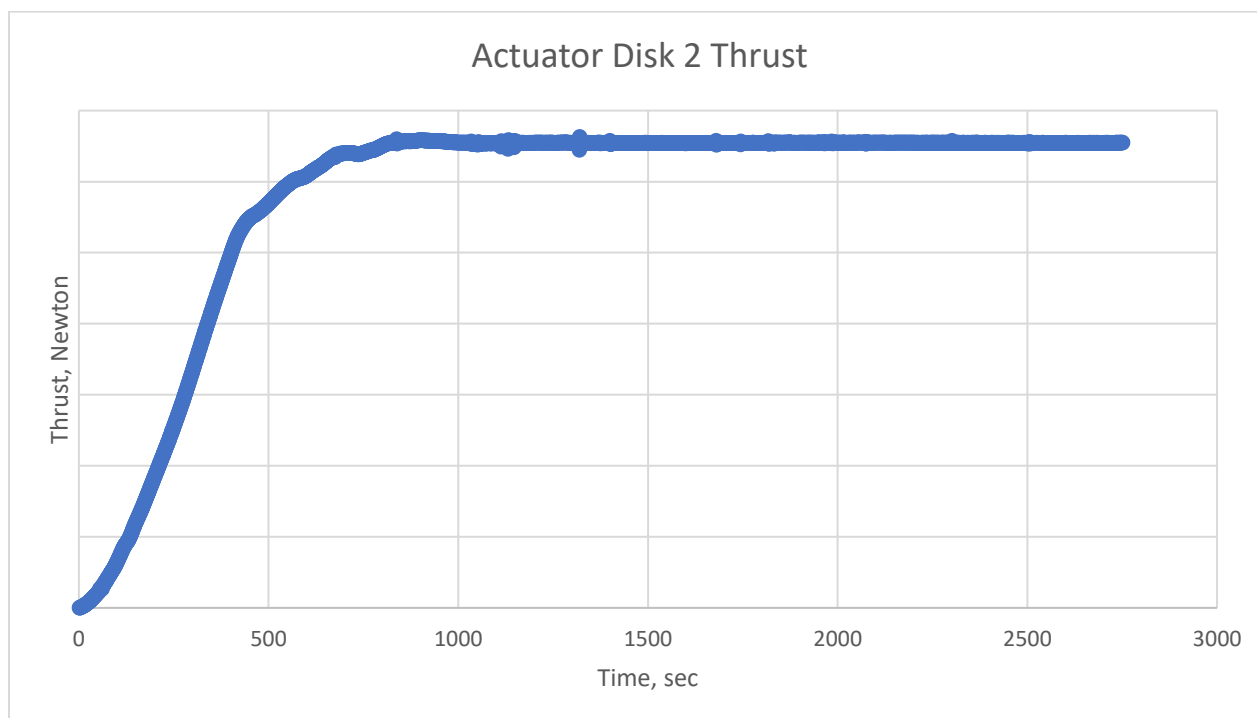


Figure 26: Actuator disk No 2 [Thrust and Torque]

From the above two pictures it can be seen that the thrust for actuator disks is also converged to a specific value. The system was automated and it could be stopped manually after 45 seconds simulation time.

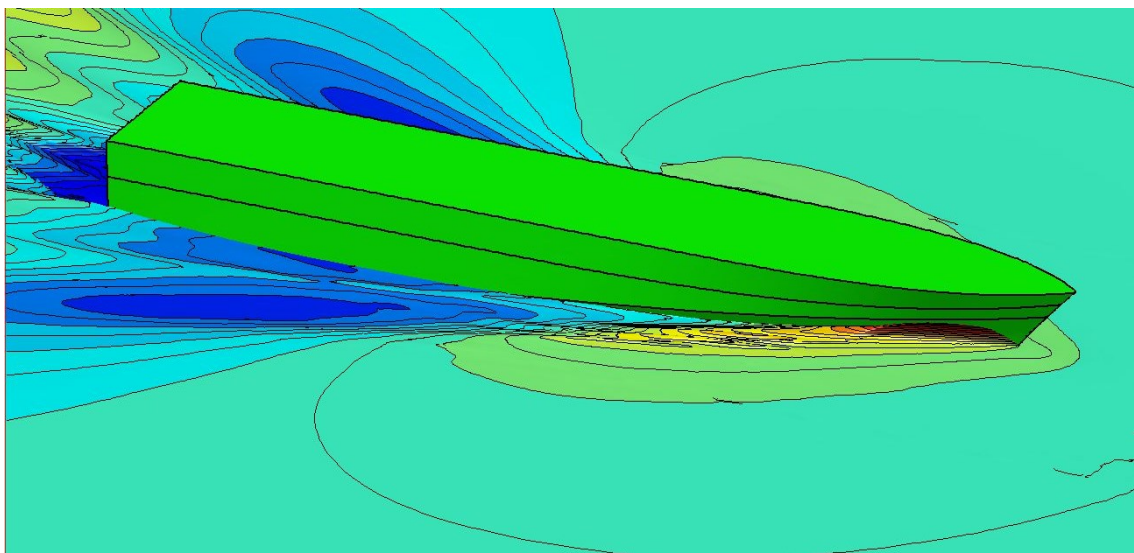


Figure 27: Free surface Elevation

From the above picture the free surface can be seen during the acceleration process. The highest bow wave elevation was recorded at X meter and the lowest stern wave recorded at Y meter. The X and Y values are confidential and was not declassified in this document.

3.5.2 Turning Circle Phase Result and Graphics

For turning circle phase, the X direction force and Y direction force, hereby titled as 'Fx' and 'Fy' respectively was obtained from the software. The surge, sway, heave, pitch, roll and yaw motion, velocity curves were also obtained. The free surface deviation and hydrodynamic pressure are also seen from the software.

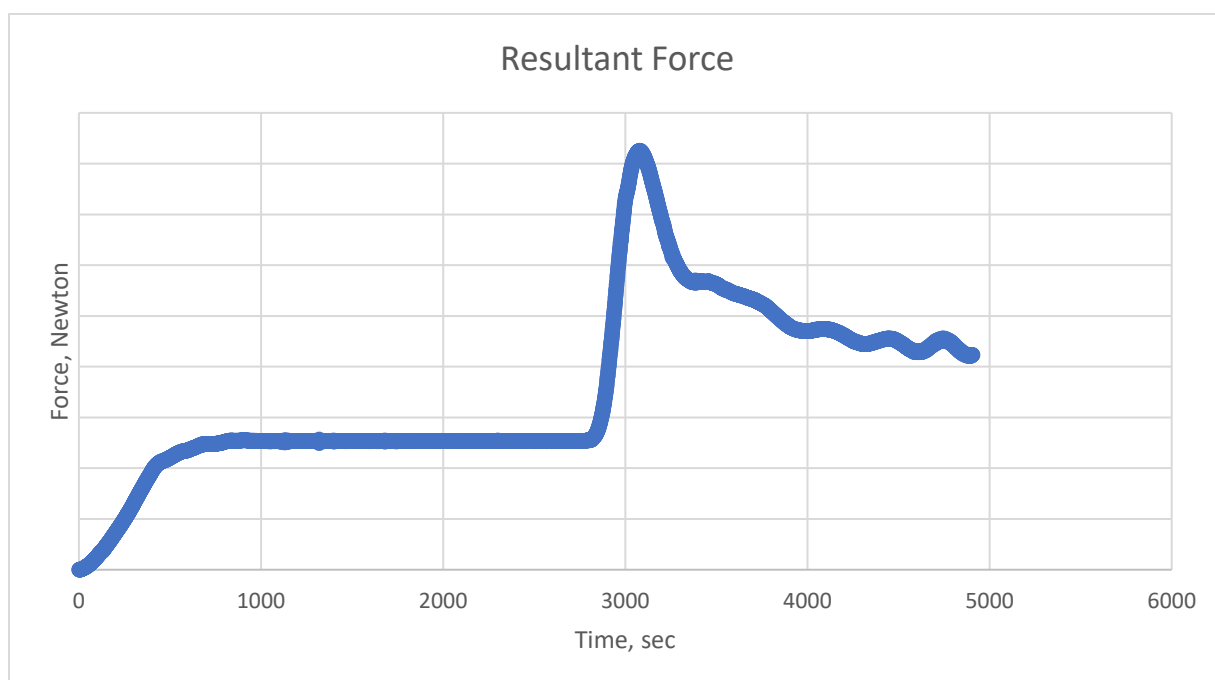


Figure 28: Resultant Force [TC]

It can be seen that the vessel experiences high resultant force during the initial turning phase. The resultant force starts to decrease soon. The reason behind this force abnormality is that the flow is not symmetric around the hull anymore. As a result, flow separation occurs and induces more translational drag component. Moreover, the rudder profile and the flow around the rudder is also changed due to turning. These are responsible for inducing more side force and hence increasing the drag.

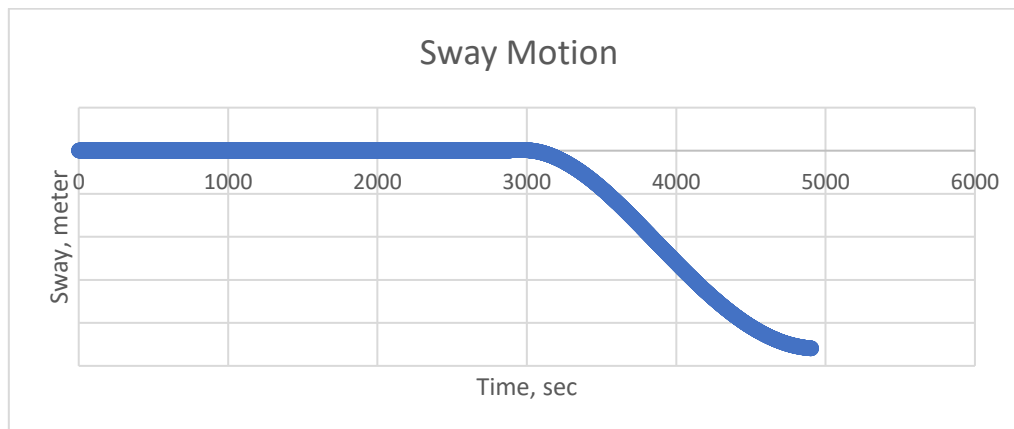


Figure 29: Sway Motion [TC]

It can be seen that the vessel has moved a significant distance in y direction. The value was not provided due to confidentiality reason. The direction seems to be changing and the surge value will be reducing. The computation was run up to 185 degrees heading to save computation cost. If a full 360 degrees circle was completed, lower value of sway will be visible afterwards as the vessel will be returning to its original trajectory.

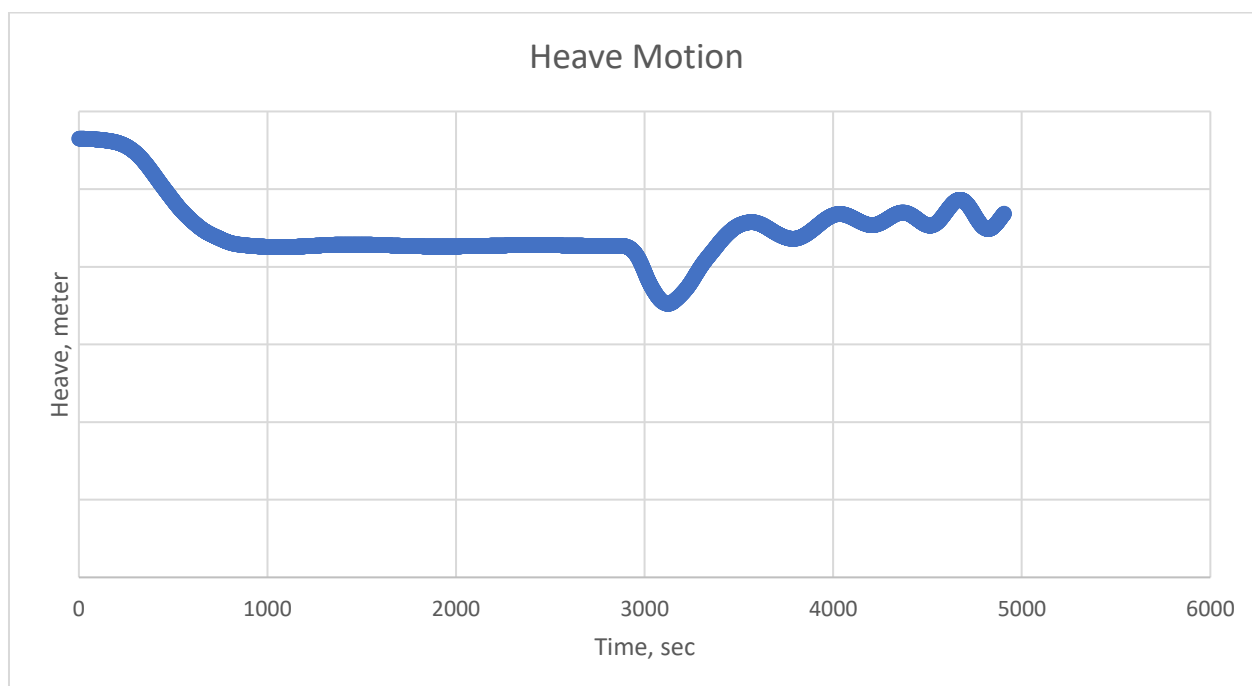


Figure 30: Heave Motion [TC]

During initial turning, the underwater profile of the vessel is changed. As a result, a new center of buoyancy will evolve. Interaction between new CB and predefined CG will cause more bodily sinkage hence a new heave equilibrium will be prominent. However, as the vessel inducing more turn, the diverging wave from the vessel is believed to be interacting with vessel. This could be the reason behind the oscillation for the heave.

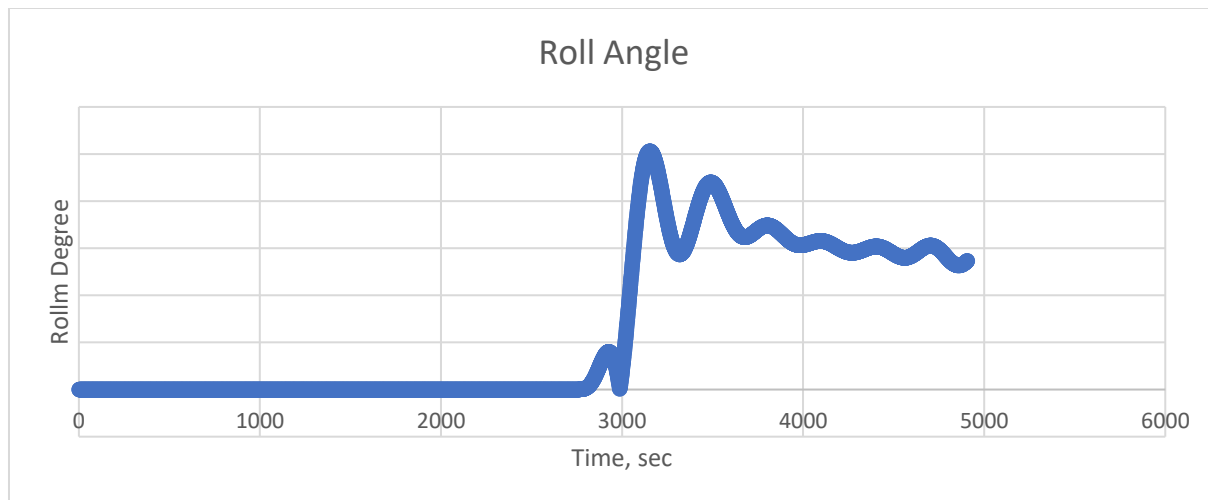


Figure 31: Roll [TC]

During initial turning, the underwater profile of the vessel is changed. An outboard angle is noticed at the very initial stage. This is due to the initial turning moment induced by the rudder. As hull moments and forces are being induce and a new equilibrium is being positioned, an inboard angle is noticed. This is plausible with the theory as the forces now have a component from “centripetal force”. A maximum inboard angle is noticed and then it reduced to a lower value. In this case, it was inboard rolling for 185 degrees heading.

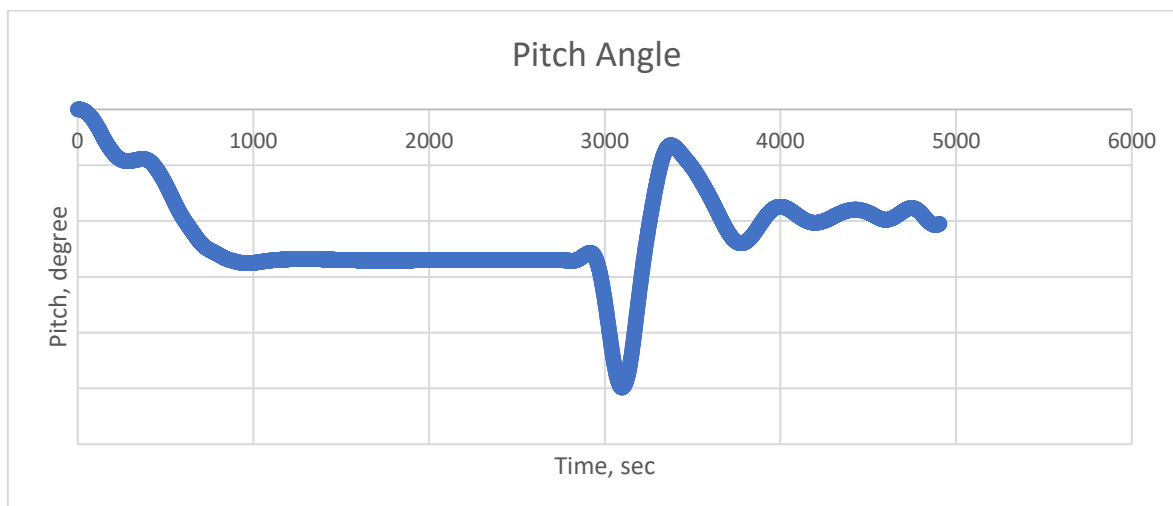


Figure 32: Pitch [TC]

During initial turning, the underwater profile of the vessel is changed. The initial disturbance caused a high pitch which also stabilizes over time.

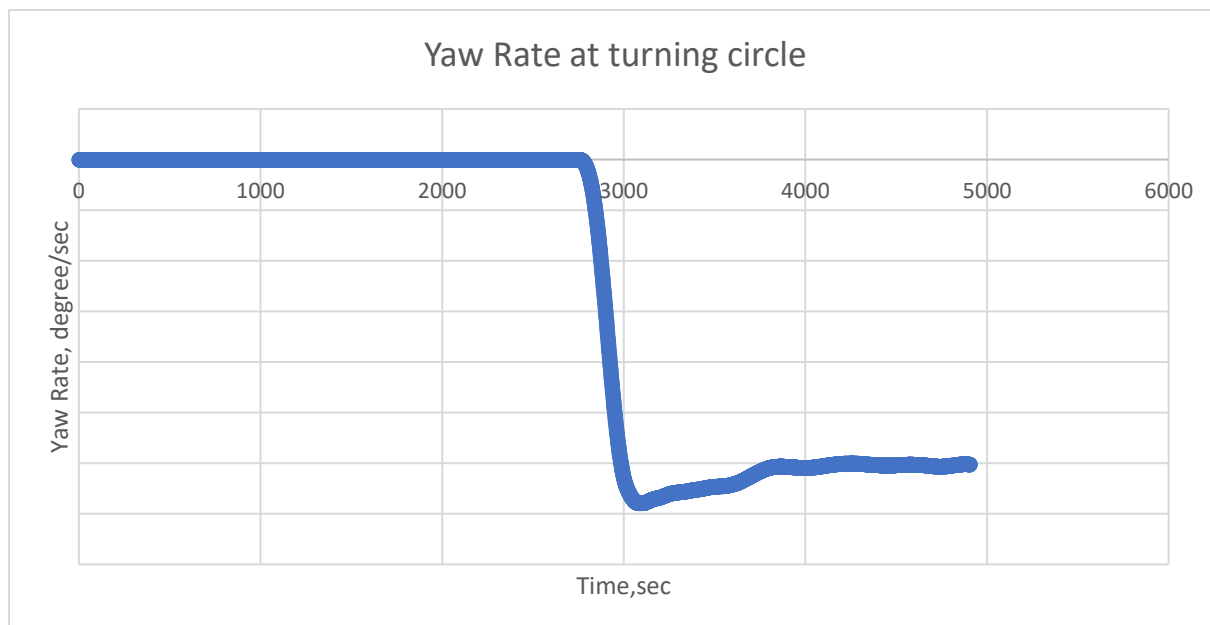


Figure 33: Yaw rate [TC]

The above picture shows yaw rate. This is the decision-making variable for the simulation. To obtain correct data feeds, a steady turning rate is required so that it can be said that the vessel is in equilibrium.

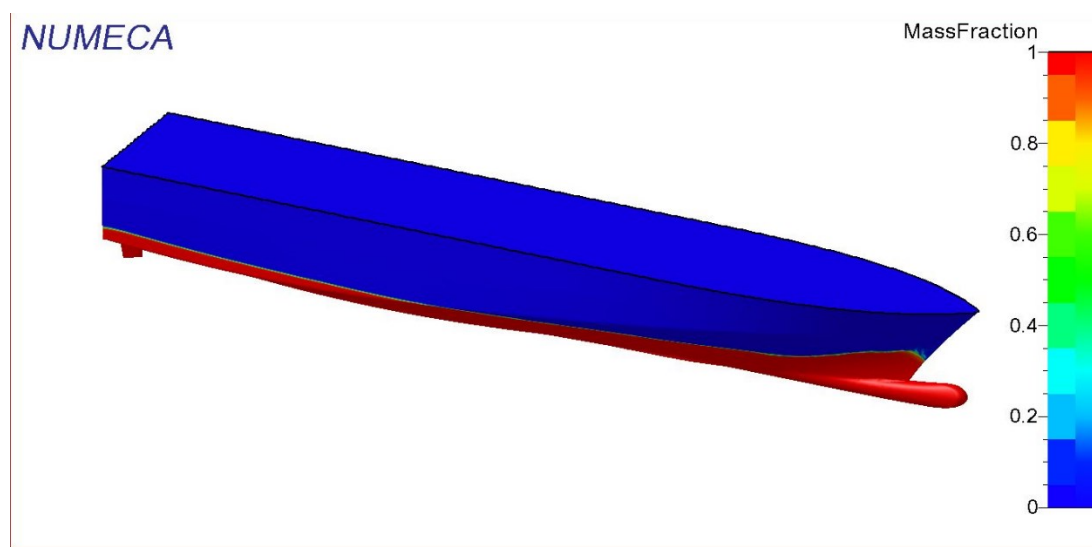


Figure 34: Mass Fraction [TC]

The above picture shows the mass fraction of the whole vessel. During bow wave creation, at the free surface layer both fluids interact. As a result, a mixture is noticed.

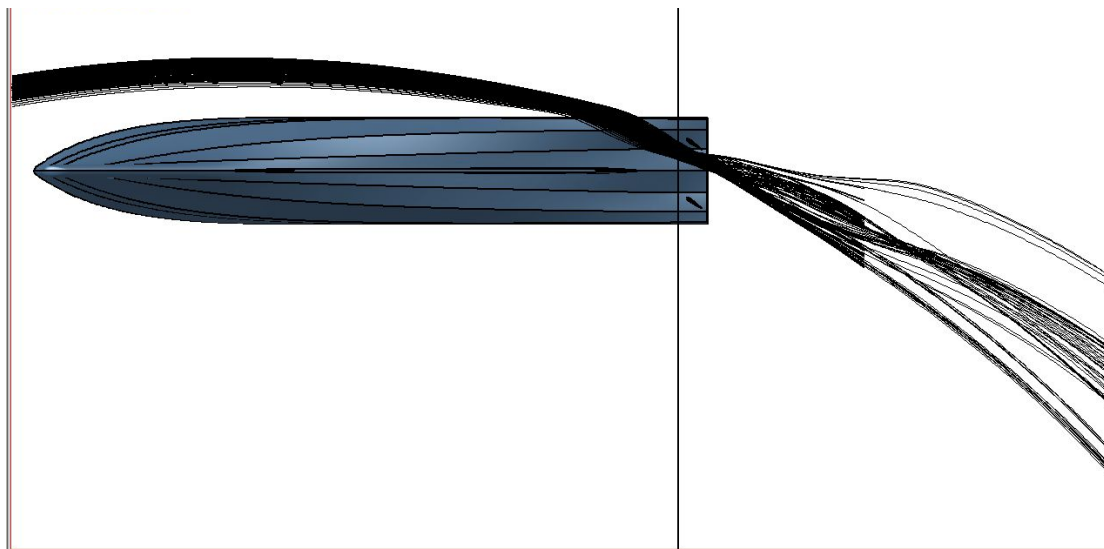


Figure 35: Relative Velocity [TC]

The above picture shows relative velocity from the top view (viewed from positive Z). It shows the path of the fluid particles during the turning maneuvering. The interaction between the rudder and the hull chine is quite interesting point of investigation for selection of steering devices.

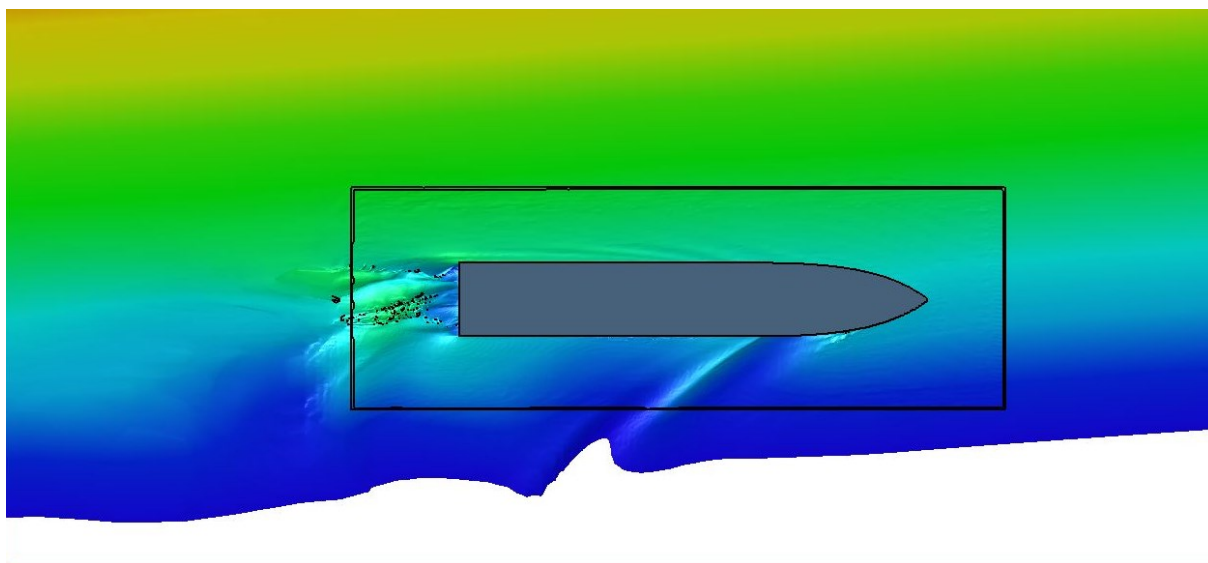


Figure 36: Free surface [TC]

The above picture shows wave elevation from the top view (viewed from positive Z). It shows the free surface during the turning maneuvering. The highest wave elevation is noticed near the background boundary. It is a far field and does not concern enough significance to analysis.

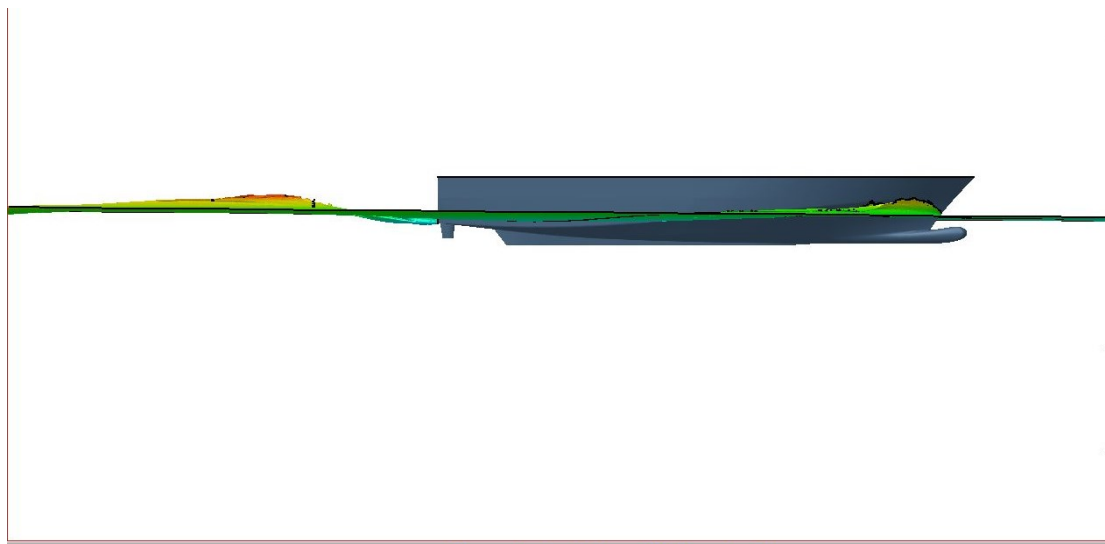


Figure 37: Free surface [TC]

The above picture shows wave elevation from the side view. It shows the free surface during the turning maneuvering. The wave elevation is noticed near the bow area creating bow wave and high-pressure wave formation is noticed just past the stern.

The table below shows the value of the imposed and solved parameters obtained throughout the simulation.

Table 8: Solved Parameter for 3 DOF and 6 DOF

Overall Computation Time for the complete simulation			
Parameter	3 DOF	6 DOF	Remarks
Surge	Classified Data (All rights reserved to Mauric)	Classified Data (All rights reserved to Mauric)	23.25 % Relative Difference
Sway			3.33 % Relative Difference
Heave			Oscillation Noticed for 6 DOF
Roll			Inboard Roll
Pitch			Pitch up
Yaw	201.04 [deg]	186 [deg]	

3.5.3 Comparison for 3 DOF and 6 DOF with Experimental Data

As mentioned earlier, a successful computation was run by solving 3 DOF during initial stage. After that another successful computation was performed solving all 6 DOF. The process was identical in each case. The computation starts with an acceleration phase to reach stable equilibrium and then the turning phase is executed by manipulating the rudder angle.

Acceleration Phase:

The acceleration phase for 3 DOF took about 2751 Time Steps to reach convergence. In real time it is about 71.52 seconds of simulation. However, acceleration phase was possible to stop earlier since it already converged at around 45 second which is about 1700 Time Step mark.

Turning Circle Phase:

The TC phase for 3 DOF took about 2100 Time Steps to reach convergence. In real time it is about 54.6 seconds of simulation. For 6 DOF took about 2155 Time Steps to reach convergence. In real time it is about 56.03 seconds of simulation.

Table 9: Computation Time

Overall Computation Time for the complete simulation			
DOF	Acc Time [Hrs.]	TC Time [Hrs.]	Total Time [Hrs.]
TC 3 DOF	30	54	84
TC 6 DOF	30	98.7	128.7
TC 6 DOF (if Acc stopped earlier)	22	98.7	120.7

The above table shows the complete time for the simulation. A 53.21 %-time increment for solving 6 DOF can be seen. However, this is not definite as it was possible to stop the acceleration phase for 6 DOF earlier. This percentage is purely based on this computation and should not be taken as a definite value. It was performed just see the duration and the variation on the results. In both cases, the vessel was turning towards starboard.

Table 10: Comparison for 3 DOF and 6 DOF

Overall Computation Time for the complete simulation			
Parameter	3 DOF	6 DOF	Remarks
Advance Relative Difference (%)	-	4.5	
Transfer Relative Difference (%)	-	3.0	
TD Relative Difference (%)	-	2.8	

The above table shows the difference on Advance, Transfer and Tactical Diameter between 3 Degrees of Freedom and 6 Degrees of Freedom. It can be seen that there are about 3 % difference on Transfer between 3 and 6 degrees of freedom, and 2.8 % difference on Tactical Diameter between 3 and 6 degrees of freedom,

Table 11: Comparison for 3 DOF and Full-Scale Trial

Overall Computation Time for the complete simulation			
Parameter	3 DOF	Full Scale	Remarks
Advance [m]	Classified Data (All rights reserved to Mauric)	Classified Data (All rights reserved to Mauric)	The TD/Lpp deviation with Full scale and Simulation is: 17.79 %.
Advance / L _{PP}			
Transfer [m]			
TD [m]			
TD / L _{PP}			
T ₉₀ [s]			
T ₁₈₀ [s]			
Velocity _{approach} [knots]			
Velocity _{steady} [knots]			
Speed Ratio			

The above table shows the difference between different parameters between 3 Degrees of Freedom and Full Scale Trial. It can be seen that there 17.8 % difference between 3 dof simulation and full-scale trial for tactical diameter.

Table 12: Comparison for 6 DOF and Full-Scale Trial

Overall Computation Time for the complete simulation			
Parameter	6 DOF	Full Scale	Remarks
Advance [m]	Classified Data (All rights reserved to Mauric)	Classified Data (All rights reserved to Mauric)	The TD/Lpp deviation with Full scale and Simulation is: 15.43 %.
Advance / L _{PP}			
Transfer [m]			
TD [m]			
TD / L _{PP}			
T ₉₀ [s]			
T ₁₈₀ [s]			
Velocity _{approach} [knots]			
Velocity _{steady} [knots]			
Speed Ratio			

The above table shows the difference between different parameters between 6 Degrees of Freedom and Full Scale Trial. It can be seen that there 15.43 % difference between 6 dof simulation and full-scale trial for tactical diameter.

3.5.4 Post Processing Results

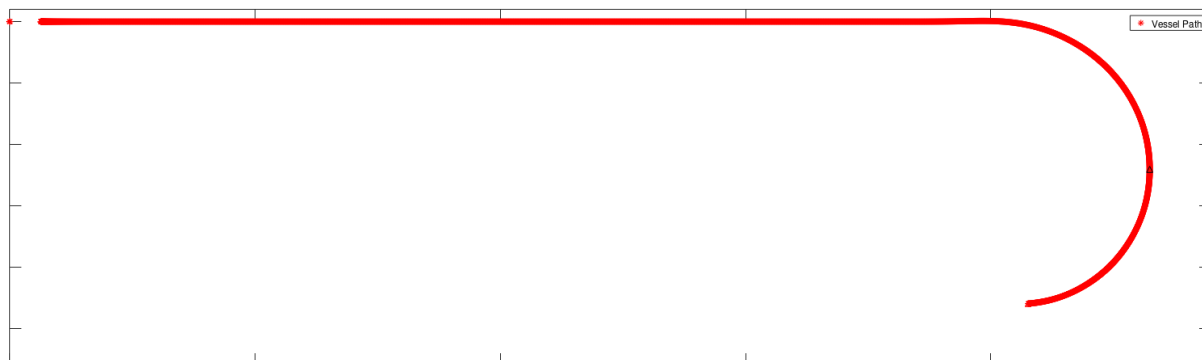


Figure 38: Vessel Trajectory [6 DoF Simulation]

From the above picture, the trajectory of the vessel is seen. This was for 6 DoF and it was computed up to 185-degree heading. Based on that, the maximum sway value and the maximum surge value are calculated but they are not disclosed due to confidentiality reason. It has to be kept in mind that the surge values are being taken from the initial approach condition.

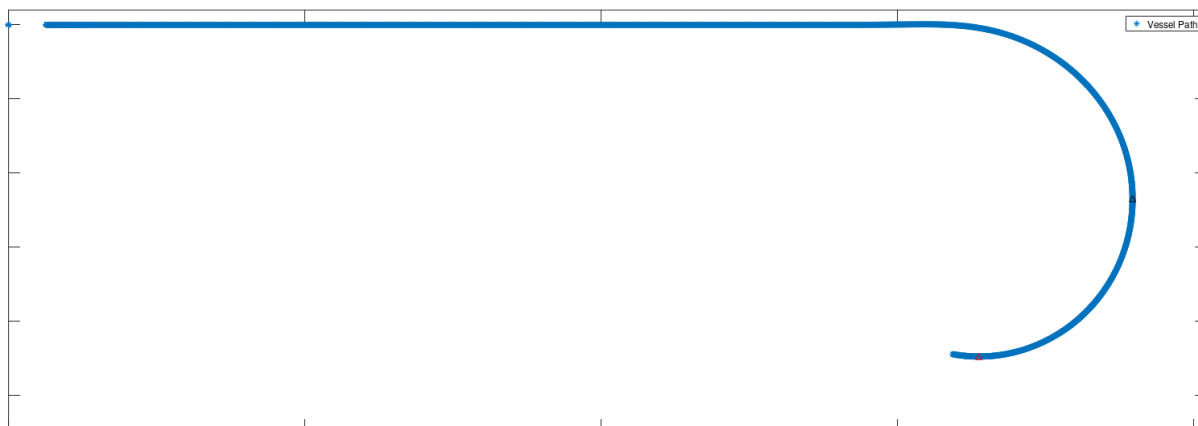


Figure 39: Vessel Trajectory [3 DoF Simulation]

From the above picture, the trajectory of the vessel is seen. This was for 3 DoF and it was computed up to 201-degree heading. Based on that, the maximum sway value and the maximum surge value are obtained but it is classified. It has to be kept in mind that the surge values are being taken from the initial approach condition.

3.5.5 Critical Analysis

The results were obtained from the simulation and then further post-processed using the Octave software. It can be seen that there are some differences between the full-scale trial and simulation. It could be associated to the three main reasons mentioned following:

- i. Hull: The hull geometry considered in the simulation is simplified without any appendages like shafting brackets, bilge keel and tunnel thruster. It is also without the physical propeller and rudder hull connecting tiller rod. The tiller rod was causing meshing issues and as a result it was removed from the hull as per the suggestion by FineMarine. In a global scale this may not be a significant issue but this is still a part of the appendages.
- ii. Speed: The fluid particle speed around the hull has a specific speed but the rudder and propeller are not at the same speed due to induced drift angle during turning and propeller side force. There will also be slip in the propeller which will reduce the velocity of the fluid particle approaching towards rudder vane. The low velocity will induce less normal force as we know the rudder normal force is as following equation [58]:

$$F_N = 0.5\rho A_R V_R^2 C_N$$

Equation 57

- iii. Environmental Factor: The real test condition could be affected by environmental factors such as wind, wave. Although the regulation states the test to be conducted in as calm water as possible. In case of simulation, it was a hypothetical ideal condition with no wind and wave. This could be affecting the result a bit as well.

3.6 Challenges and Computation Error

There was some computational error throughout the total simulation process. The end results can be seen here but it was full of challenges to do a simulation with overset domains. The computations were noticed to be diverged or failed. The two main computation errors that was prompting frequently are mentioned below:

a. Diverging Computation:

The diverging computation occurs when the residual is too high and become an invalid number which cause the computation to stop for numerical instability. The most common symptoms that can occur during this stage is “failing after a specific time step or iteration number” or “Incorrect cell location value”. The solution for this type of failure is to assess the correct inertia matrix, rechecking the hydrostatic position of the vessel and rechecking the mesh.

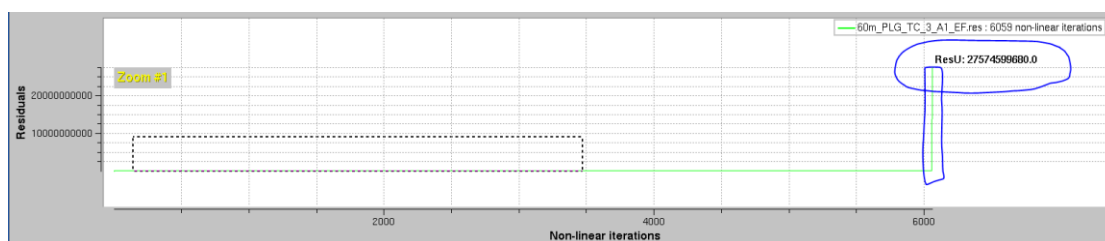


Figure 40: Residual becoming invalid

b. Grid matching error:

The grid matching error can also occur when the residual is too high and become an invalid number which cause the computation to stop for numerical instability. The most common symptoms that can occur during this stage is “failing after a specific time step or iteration number” or “Grid Location Error” or “Failed to interpolate”. The solution for this type of failure is to assess the correct target cell size and rechecking the mesh refinement.

Chapter 4 Conclusion and Recommendation

In this chapter, a summary is provided about the calculation procedure, obtained result and the limitations as well as possibilities to expand the research work further. The findings written here on the report are based on the bibliographical research for the high-speed vessels. It is evident that there could be numerous variations for the vessel and as so the research will also have a different aspect in case of vessel design.

4.1 Conclusion

As a summary of the overall work conducted in the thesis, it can be stated that the task was an interesting topic to work with in the aspect of industry as well as in the aspect of a research. With the current methodology, a maximum of 15.4% closer result to the experimental data was achieved for tactical diameter. The study is highly significant for marine vessel design industry since it is possible to predict the turning circle with appropriate and acceptable deviation. From the simulation, it is also possible to find out the high-pressure formation area on the hull or the area of flow separation as well as the location of the free surface on the hull. All of these can help a naval architect to understand the vessel dynamics more accurately and change the hull form if required.

Another aspect of this thesis and internship work can be viewed on the academic research point of view. The study can be further extended towards the mathematical model development for more accurate prediction with less error percentage. Although, overset grid technique is already being used for overlapping domains by experts, the possibility to extend this technique is endless. It can be used with acceleration methods to speed up computation. The cell-to-cell data exchange method can also be an interesting arena to work on.

4.2 Limitations

While studying for the theoretical bibliography for high-speed vessel maneuvering, a number of limitations were found. Although they do not have a large effect on the study but it would be more evident to have the possibility of conducting the research with these limitations skipped. They are mentioned below in a nut shell:

1. Inadequate model test or real scale experimental data.
2. Adding an irregular wave of 2nd or 3rd order.
3. Inadequate empirical formulation to make an initial prediction.
4. Although the turning circle diameter test is carried out at as calm water as possible. However, the effect of heavy wind in case of emergency collision avoidance maneuvering is not known accurately. These are something that could require further investigation.

4.3 Recommendations

The task of finding out the turning circle is computationally demanding. The task carried out in the Master's thesis internship was conducted as a part of a gradual work progress. The turning circle and crash stop for a bare mono hull ship with propeller was done. Instead of actual physical propeller in the model, a numerical model known as "actuator disk" is used. However, there are a lot of approaches for improvement. The future work can be done on two aspects. The first and the most important aspect can be to test out different types of vessels with different configuration. Some of them are listed below:

1. Addition of another hull or catamaran configuration and with consideration of hull-to-hull interaction.
2. Addition of Appendages on the hull.
3. Addition of an azimuth thruster or a waterjet as propulsor device.
4. Variation in the number of propeller and rudder configuration.
5. Analysis with different type of rudders. Based on research conducted in Korea, it was concluded that twisted rudder is more effective for large size high speed vessels. It could be an interesting application for the research.

The second approach could be based on the computation time. The target at this stage could be to improve the way to speed up the computation itself. The following areas could be seen as an interest for further expansion of this research.

1. Overset grid cell data exchange method.
2. Faster convergence with lowest possible iteration number.

Chapter 5 Reference

- [1] Kim, Inchul & Chae, Chong & Lee, Soyeong. (2020). Simulation Study of the IAMSAR Standard Recovery Maneuvers for the Improvement of Serviceability.
- [2] Maritime Safety Committee, 2-13 December 2002, "Standards for Ship Manoeuverability ", MSC Meeting 76th Session, London, United Kingdom.
- [3] International Towing Tank Conference, 2008, "Testing and Extrapolation methods maneuverability free running model tests", Proceedings of 25th ITTC, Fukuoka, Japan, Vol. 1
- [4] International Towing Tank Conference, 2017, "Full Scale Maneuvering Trials", Proceedings of 28th ITTC, Wuxi, China, Vol. 1
- [5] International Towing Tank Conference, 2014, "Evaluation and Documentation of HSMV", Proceedings of 27th ITTC, Copenhagen, Denmark, Vol. 1
- [6] International Towing Tank Conference, 2014, "Validation of Maneuvering simulation models", Proceedings of 27th ITTC, Copenhagen, Denmark, Vol. 1
- [7] International Towing Tank Conference, 2017, "Guideline on the use of RANS tools for maneuvering prediction", Proceedings of 28th ITTC, Wuxi, China, Vol. 1
- [8] Guide for Vessel Maneuverability, American Bureau of Shipping, March 2006.
- [9] Szlangiewicz, Tadeusz & Żelazny, Katarzyna. (2018). Mathematical Model for Predicting the Ship Speed in the Actual Weather Conditions on the Planned Ocean Route. *New Trends in Production Engineering*. 1. 105-112. 10.2478/ntp-2018-0013.
- [10] Bowles, Jeffrey. Turning Characteristics and Capabilities of High-Speed Monohulls, "THE THIRD CHESAPEAKE POWER BOAT SYMPOSIUM.", Annapolis, Maryland, June 2012.
- [11] Lewandowski, Edward M., *The Dynamics of Marine Craft*, Singapore, World Scientific Publishing Co. Pte. Ltd., 2004.
- [12] Wei Zhang, Zao-Jian Zou, De-Heng Deng, A study on prediction of ship maneuvering in regular waves, *Ocean Engineering*, Volume 137, 2017, Pages 367-381, ISSN 0029-8018.
- [13] Faltinsen, Odd M., *Hydrodynamics of High-Speed Marine Vehicles*, Cambridge, Cambridge University Press, 2005.
- [14] Kreuzer, E. J., & Sichertmann, W. M. (2005). Slender body theory approach to nonlinear ship motions. 20th IWWFEB, Spitsbergen, Norway.

- [15] J.P Hooft, The cross-flow drag on a maneuvering ship, *Ocean Engineering*, Volume 21, Issue 3, 1994, Pages 329-342, ISSN 0029-8018.
- [16] KIJIMA, K . , NAKIRI, Y . , TANAKA, S. and FURUKAWA, Y . 1990. On a numerical simulation for predicting ship manoeuvring performance. 19th ITTC, Madrid, Spain.
- [17] Cao, Zhiwei, Shasha Gao and Songlin Yang. "Roll Motion Analysis of a High-Speed Mono-hull Ship.", *Advances in Engineering Research*, Volume 141, 2017.
- [18] Taylan, Metin, "Nonlinear roll motion of ships in beam waves", *Bulletin of the Technical University of Istanbul*, Volume 49, pp 459 -479, 1996.
- [19] Taylan, Metin, "Effect of Forward Speed on Ship Rolling and Stability" *Mathematical and Computational Applications* 9, no. 2: 133-145, 2004.
- [20] Haruzo Eda, Maneuvering performance of high-speed ships with effect of roll motion, *Ocean Engineering*, Volume 7, Issue 3, 1980, Pages 379-397, ISSN 0029-8018.
- [21] Yang, Wang Lin, Song Lin Yang, Sheng Zhang, and Tian Yu Ma. "The System Identification Analysis of the Rolling Motion Model for the Unmanned Boat." *Advanced Materials Research*, Volume 1037, Trans Tech Publications, Ltd., October 2014.
- [22] Bikdash, M., Balachandran, B. & Navfeh, A. Melnikov analysis for a ship with a general roll-damping model. *Nonlinear Dyn* 6, 101–124 (1994).
- [23] Yasukawa, H., Ishikawa, T. & Yoshimura, Y. Investigation on the rudder force of a ship in large drifting conditions with the MMG model. *J Mar Sci Technol* 26, 1078–1095 (2021).
- [24] Yasuo Yoshimura, Yumiko Masumoto, Hydrodynamic Force Database with Medium High Speed Merchant Ships Including Fishing Vessels and Investigation into a Manoeuvring Prediction Method, *Journal of the Japan Society of Naval Architects and Ocean Engineers*, 2011, Volume 14, Pages 63-73, Released March 09, 2012, Online ISSN 1881-1760, Print ISSN 1880-3717.
- [25] Delefortrie, G., Van Hoydonck, W. & Eloot, K. Forces and Torque acting on a Rudder while Manoeuvring. *J Mar Sci Technol* (2021).
- [26] Abramowski, T. (2005). Prediction of propeller forces during ship maneuvering. *Journal of Theoretical and Applied Mechanics*, 43, 157-178.
- [27] Dai, K. I Li, Y. (2021). EXPERIMENTAL AND NUMERICAL INVESTIGATION ON MANEUVERING PERFORMANCE OF SMALL WATERPLANE AREA TWIN HULL. *Brodogradnja*, 72 (2), 93-114.

- [28] Moreno, Jorge & Sierra, Eddy & González, Víctor. (2011). Ship maneuverability: full-scale trials of colombian Navy Riverine Support Patrol Vessel. *Ciencia y tecnología de buques*. 5. 69. 10.25043/19098642.52.
- [29] Oldfield et al., Prediction of warship maneuvering coefficient using CFD, Defence Research and Development Canada, Valcartier Research Centre, Canada, Report Number: DRDC-RDDC-2015-P169, 2015.
- [30] Bhattacharyya, Rameswar. "Dynamics of Marine Vehicles." (1978).
- [31] Schoop-Zipfel, Karl J., "Efficient Simulation of Ship Maneuvers in Waves", PhD Thesis, Technischen Universität Hamburg, Hamburg 2016.
- [32] Mucha, Philipp. "On Simulation-based Ship Maneuvering Prediction in Deep and Shallow Water", PhD Thesis, Universität Duisburg-Essen, Duisburg 2017.
- [33] Matusiak, J., & Stigler, C. (2012). "Ship motion in irregular waves during a turning circle manoeuvre". The 11TH International Conference on the Stability of Ships and OCEAN Vehicles, Athens, 23-28 September 2012 (pp. 291-298). National Technical University of Athens, School of Naval Architecture and Marine Engineering.
- [34] Khanfir, S., Hasegawa, K., Nagarajan, V. et al. Manoeuvring characteristics of twin-rudder systems: rudder-hull interaction effect on the manoeuvrability of twin-rudder ships. *J Mar Sci Technol* 16, 472–490 (2011).
- [35] Park, Ilryong, Bugeun Paik, Jongwoo Ahn, and Jein Kim. 2021. "The Prediction of the Performance of a Twisted Rudder" *Applied Sciences* 11, no. 15: 7098. <https://doi.org/10.3390/app11157098>
- [36] Katayama, Toru & Taniguchi, Tomoki & Fujii, Haruna & Ikeda, Yoshiho. (2009). DEVELOPMENT OF MANEUVERING SIMULATION METHOD FOR HIGH-SPEED CRAFT USING HYDRODYNAMIC FORCES OBTAINED FROM MODEL TESTS, 10th International Conference on Fast Sea Transportation FAST 2009, Athens, Greece, October 2009.
- [37] Yasukawa, H., Yoshimura, Y. Introduction of MMG standard method for ship maneuvering predictions. *J Mar Sci Technol* 20, 37–52 (2015).
- [38] Aslan, Nazmi. "MANEUVERABILITY ESTIMATION OF HIGH-SPEED CRAFT", Master's Thesis, Naval Postgraduate School, June 2015.
- [39] Bhawsinka, Karan. "Maneuvering Simulation of displacement type ship and planning hull", Master's Thesis, Memorial University of Newfoundland, November 2011.
- [40] Liu, J., Hekkenberg, R., & Rotteveel, E. (2014). A proposal for standard manoeuvres and parameters for the evaluation of inland ship manoeuvrability.

- [41] Wang, Jianhua and Decheng Wan. "CFD study of ship stopping maneuver by overset grid technique." *Ocean Engineering* 197 (2020): 106895.
- [42] K Varyani & P Krishnankutty (2009) Stopping manoeuvre of high speed vessels fitted with screw and waterjet propulsion, *Journal of Marine Engineering & Technology*, 8:1, 11-19.
- [43] Park, Jong-Yong, et al. "Study on Stopping Ability of a Ship Equipped with Azimuth Propeller." *Journal of Ocean Engineering and Technology*, vol. 34, no. 1, The Korean Society of Ocean Engineers, 28 Feb. 2020, pp. 13–18.
- [44] Oneto, L., Andrea Coraddu, Paolo Sanetti, Olena Karpenko, Francesca Cipollini, Toine Cleophas and D. Anguita. "Marine Safety and Data Analytics: Vessel Crash Stop Maneuvering Performance Prediction." ICANN (2017).
- [45] Yabuki, Hideo, Yasuo Yoshimura, Tsuyoshi Ishiguro and Michio Ueno. "Turning motion of a ship with single CPP and single rudder during stopping maneuver under windy condition." *Conference Proceedings, MARSIM, Netherlands, 2006.*
- [46] Sun, Chenguang, Wang, Jianhua, and Decheng Wan. "Numerical Simulations of Ship Stopping Maneuver with Reversing Propeller." Paper presented at the The Thirteenth ISOPE Pacific/Asia Offshore Mechanics Symposium, Jeju, Korea, October 2018.
- [47] Ming, Li, J. Liu and Song Yang. "A New Method on Calculation of Vessels Stopping Distance and Crash Stopping Distance." *Advanced Materials Research* 779-780 (2013): 800 - 804.
- [48] Duman, Suleyman and Sakir Bal. "Prediction of the acceleration and stopping manoeuvres of a bare hull surface combatant by closed-form solutions and CFD." *Ocean Engineering* 235 (2021).
- [49] Tani, H. "The Reverse Stopping Ability of Supertankers." *Journal of Navigation* 21, no. 2 (1968): 119–54. doi:10.1017/S0373463300030290.
- [50] Norrby, Ralph A., "A STUDY OF CRASH STOP TESTS WITH SINGLE SCREW SHIPS", Report 119 of the Chalmers University of Technology, Division of Ship Hydromechanics, Gothenburg, Sweden, 1972.
- [51] Gan, Langxiong, Liangming Li, Yuangzhou Zheng and Baogang Zhang. "A New Method for Accurate Prediction of Ship's Inertial Stopping Distance." *Research Journal of Applied Sciences, Engineering and Technology* 6 (2013): 3437-3440.
- [52] Okamoto, H. et al. 'Stopping Abilities of Ships Equipped with Controllable Pitch Propeller'. *International Shipbuilding Progress*, vol. 21, no. 234, pp. 40-50, 1974.

- [53] Ueno, Michio & Suzuki, Ryosuke & Tsukada, Yoshiaki. (2017). Estimation of stopping ability of full-scale ship using free-running model. *Ocean Engineering*, 130, 260-273.
- [54] Harvald, Sv.Aa. 'Factors Affecting the Stopping Ability of Ships', *International Shipbuilding Progress*, vol. 23, no. 260, pp. 106-121, 1976.
- [55] Liu, H, Ma, N, & Gu, X. "Maneuvering Prediction of a VLCC Model Based on CFD Simulation for PMM Tests by Using a Circulating Water Channel." *Proceedings of the ASME 2015 34th International Conference on Ocean, Offshore and Arctic Engineering*. Volume 2: CFD and VIV. St. John's, Newfoundland, Canada. May 31–June 5, 2015. V002T08A041. ASME.
- [56] Karim, Md. Mashud et al. "PERFORMANCE OF SST K- ω TURBULENCE MODEL FOR COMPUTATION OF VISCOUS DRAG OF AXISYMMETRIC UNDERWATER BODIES." *International Journal of Engineering* 24 (2011): 139-146.
- [57] Darvish, M. (2015). Numerical and experimental investigations of the noise and performance characteristics of a radial fan with forward-curved blades.
- [58] Liu, J., Quadvlieg, F., & Hekkenberg, R. (2016). Impacts of the rudder profile on manoeuvring performance of ships. *Ocean Engineering*, 124, 226-240.

Appendices: Octave Code

```

%% Calculation Script for Vessel "Advance", "Transfer" and "Tactical Diameter"

clear all
close all

printf("***Calculation Script for Vessel Advance, Transfer and Tactical Diameter***\n\n");

% Full Scale test trial data (change in "user input" section when required)
% Starboard Turn:
% TD = 270 [m] & Time = 1 min 31 sec
% Port Turn:
% TD = 262 [m] & Time = 1 min 35 sec

% Data reading for the hull
data_Hull = 'Mvt_Hull.dat';
m = dlmread(data_Hull);

% User Input:

ATS = 2751;      % Acceleration Phase Completed Time Step (To be changed by user as required)
Lpp = 56.59;    % Full scale length between perpendiculars (To be changed by user as required)
TS = .026;     % Time Step size (To be changed by user as required)
tv = 10.802;   % Target Velocity (m/s) from which the speed will be reduced in inertia stop
Full_Td = 270; % Full Scale TD on Starboard side

% Simulation Time
t = ATS*TS;
time = m(:,1); % Be sure to check the column number in dat file
idnumber = find(time==t);

% Heading angle find (angle in dat file are in radian)
% (-) sign is just for direction as the vessel turned starboard

P = m(:,5);
PQ1 = -1.58; % Put 0.01 digit more than the value = -90*3.1416/180;
PQ2 = -3.15; % Put 0.01 digit more than the value = -180*3.1416/180;

[k1,dist] = dsearchn(P,PQ1);
[k2,dist] = dsearchn(P,PQ2);

k11 = k1-1;
k22 = k2-1;

% Surge and Sway find

surge = m(:,2); % Be sure to check the column number in dat file
sway = m(:,3); % Be sure to check the column number in dat file
surgemax = max(surge);
swaymax = max(sway);
surgemin = min(surge);
swaymin = min(sway);

% Plotting the general data
figure(1)

plot(surge,sway,'*');
axis([surgemin surgemax swaymin swaymax],"equal");
%axis([surgemin surgemax swaymin swaymax]);
% Plotting the max point for surge and sway

hold on
[surge_max,idx] = max(surge);
plot(surge_max, sway(idx), '^k');

[sway_min,idxn] = min(sway);
plot(surge(idxn), sway_min, '^r');
h = legend('Vessel Path', sprintf(' Surge Value = %0.3f meter',surge_max),sprintf(' Sway Value = %0.3f meter',sway_min));
set(h,'FontSize',12);

% Label and Titling for the Data

title ("Vessel Motion: Surge vs Sway for the Turning Radius Motion");
xlabel ("Surge Distance (m)");
ylabel ("Sway Distance (m)");
xlim([0, (surgemax+50)]);
ylim([swaymin-50, 10]);

```



```

% Advance Calculation:
Advance = surge(k11)-surge(idnumber);
printf("\nThe value of Advance is: %0.2f Meter.\n\n",Advance);

% Advance to LPP Ratio:
ratio_1 = Advance/Lpp;
printf("The ratio of Advance & Lpp is: %0.2f.\n\n",ratio_1);

% Transfer Calculation:
Transfer = sway(idnumber)-sway(k11);
printf("The value of Transfer is: %0.2f Meter.\n\n",Transfer);

% Tactical Diamter Calculation:
Td = sway(idnumber)-sway(k22);
printf("The value of Tactical Diamter is: %0.2f Meter.\n\n",Td);

% Tactical Diamter to LPP Ratio:
ratio_2 = Td/Lpp;
printf("The ratio of Tactical Diamter & Lpp is: %0.2f.\n\n",ratio_2);

% Approach Speed Calculation:
V_x = m(:,6); % Be sure to check the column number in dat file
Ap_Vel = V_x(idnumber);
Ap_Vel_Kn = Ap_Vel*1.94384; % m/s to knot conversion
printf("The Approach speed is: %0.2f m/s and %0.2f Knots.\n\n",Ap_Vel,Ap_Vel_Kn);

% Time for 90 Degree and 180 Degree Calculation:

t_90 = time(k11);
t_180 = time(k22);
printf("The time for 90 Degree turn is: %0.1f s.\n\n",t_90);
printf("The time for 180 Degree turn is: %0.1f s.\n\n",t_180);

%% Steady State Speed:

YR=m(:,9);
steady_rate_turn = -.0589; % Check from FineMarine and Convert to Radian = -3.45*3.1416/180;
[k3,dist] = dsearchn(YR,steady_rate_turn);

l = size(V_x);
rownumber = l(1,1);
V_y=m(:,7); % Be sure to check the column number in dat file

##requiredvalue=300; % shows the last x data set. x = user input (To be changed by user as required)
##target= rownumber-requiredvalue;
V_x_new = m(k3:end,6);
V_y_new = m(k3:end,7);
V = ((V_x_new).^2+(V_y_new).^2).^0.5;

Std_Vel = V(end:end);
Std_Vel_Kn = Std_Vel*1.94384;
printf("The steady speed is: %0.2f m/s and %0.2f Knots.\n\n",Std_Vel,Std_Vel_Kn);

%% Loss of Speed:
ratio_3 = Std_Vel/Ap_Vel;
printf("The ratio of steadyspeed & approach speed is: %0.2f.\n\n",ratio_3);

% Finding the percentage of deviation with simulation and full scale data

ratio_21 = Full_Td/Lpp;
printf("The ratio of Tactical Diamter & Lpp for Full scale ship is: %0.2f.\n\n",ratio_21);

perc= ((abs(ratio_21-ratio_2))/ratio_21)*100;

printf("The TD/Lpp deviation with Full scale and Simulation is: %0.2f %%\n\n",perc);

```